STRUCTURE-PRESERVING WEIGHTED BDF2 METHODS FOR ANISOTROPIC CAHN-HILLIARD MODEL: UNIFORM/VARIABLE-TIME-STEPS

MENG LI[*], JINGJIANG BI[†], AND NAN WANG[‡]

Abstract. In this paper, we innovatively develop uniform/variable-time-step weighted and shifted BDF2 (WS-BDF2) methods for the anisotropic Cahn-Hilliard (CH) model, combining the scalar auxiliary variable (SAV) approach with two types of stabilized techniques. Using the concept of G-stability, the uniform-time-step WSBDF2 method is theoretically proved to be energy-stable. Due to the inapplicability of the relevant G-stability properties, another technique is adopted in this work to demonstrate the energy stability of the variable-time-step WSBDF2 method. In addition, the two numerical schemes are all mass-conservative. Finally, numerous numerical simulations are presented to demonstrate the stability and accuracy of these schemes.

Key words. Uniform-time-step scheme, Variable-time-step scheme, Weighted and shifted BDF2 method, G stability, Energy stability

AMS subject classifications. 65N30, 65N06, 65N12

1. Introduction. As the typical phase-field, the Cahn-Hilliard (CH) equation, initially introduced to describe phase separation in binary alloys, is pivotal in materials science, especially for elucidating the qualitative features of two-phase systems under conditions of isotropy and constant temperature. Recently, the CH model has found widespread applications beyond its initial purpose, extending to surface diffusion of adatoms in stressed epitaxial thin films [1, 2, 3], dealloying in corrosion processes [4], vesicle dynamics [5], tumor growth [6, 7], multiphase fluid flow [8, 9, 10], bacterial films formation [11] and image processing [12, 13, 14]. More applications and numerical methods about the phase-field model can refer to Refs. [15, 16, 17, 18].

The anisotropic CH equation, proposed by Torabi et al. [19, 20], aims to describe the phenomenon of faceted pyramid formation on nanoscale crystal surfaces. In the anisotropic system, there exists a term $\gamma(\nabla\phi/|\nabla\phi|)$ that changes its sign as $|\nabla\phi|$ is close to zero, leading to severe oscillations and posing significant challenges to the development of algorithms for this system. In [19, 20], fully-implicit methods were employed to handle the nonlinear terms in the anisotropic CH system. However, the methods lack the proof of energy stability, and are computationally expensive due to the iterative requirement of the implicit schemes. In [21, 22], using stabilization technique, the Shen et al. established energy stable schemes for the isotropic and anisotropic CH models. All the nonlinear terms are explicitly handled by these schemes, which significantly enhances computational efficiency. However, the proof of energy stability only limits to the isotropic case. Yang et al. [23, 24] developed second-order stabilized scalar auxiliary variable (SAV) method and stabilized invariant energy 1uadratization (IEQ) method for the anisotropic CH equation, and demonstrated the energy stability of the schemes. As a development of [23], the first contribution of this work is the construction of uniform-time-step weighted and shifted BDF2 method integrated with the SAV approach for the anisotropic CH model, and derive the mass conservation and energy stability of the numerical scheme by applying the property of G-stability [25]. The work [23] is a special case of this paper, with the weighted parameter $\theta = 1$. Nonetheless, there exist substantial differences in the theoretical analytical approaches.

---

[*]School of Mathematics and Statistics, Zhengzhou University, Zhengzhou 450001, China. Email: li-meng@zzu.edu.cn.

[†]School of Mathematics and Statistics, Zhengzhou University, Zhengzhou 450001, China.

[‡]School of Mathematics and Statistics, Zhengzhou University, Zhengzhou 450001, China. Corresponding author: nwang@zzu.edu.cn.

In recent years, variable-time-step methods are popular to solve nonlinear partial differential equations (PDEs) in physical problems.Compared with the uniform temporal mesh for PDEs, variable-time-step methods and adaptive time-stepping techniques [26, 27, 28, 29, 30, 31] could better capture the multi-scale behaviors of the solutions in long time simulation and improve the computational efficiency under the same accuracy of numerical schemes. For variable-step BDF2 method, Grigorieff [32] proved that the zero-stability of this method for ODEs under the adjacent time step ratio $\gamma_{n+1} := \tau_{n+1}/\tau_n < 1 + \sqrt{2}$. In [33], Becker conducted a rigorous stability and convergence analysis of the variable-step BDF2 scheme for linear parabolic PDEs under the restriction $\gamma_n < (2 + \sqrt{13})/3 \approx 1.8685$. Chen at el. [34] studied the numerical scheme for CH model under the time step ratio $\gamma_n < 3.561$. Liao and Zhang [35] by using discrete orthogonal convolution (DOC) kernel technology, they studied the condition with $0 < r_k \leq 4.864$. Zhang and Zhao [36] obtained a new adjacent time-step ratio $0 < r_k \leq r_{\max} - \delta$ for any small constant $0 < \delta < r_{\max} \approx 4.8645$ by using the properties of DOC kernel and discrete complementary convolution (DCC) kernel. Recently, Hou and Qiao [37] proposed a variable-time-step BDF2 SAV scheme to solve the phase field crystal equation under the maximum time-step ratio $0 < r_{\max} \leq 4.864$. Interested readers can refer to [31, 35, 38, 39, 40, 41, 42, 43, 44, 45] for the variable-time-step methods applied to the divergent models, including parabolic equation, phase-field model and nonlinear Ginzburg-Landau equation. Up to now, there exists no work focusing on the variable-time-step methods for the anisotropic CH system, which is another contribution of this work.

To sum up, the main contributions of this work include:

(i) This work applies the uniform-time-step WSBDF2 method to solve the anisotropic CH model. We extend the BDF2 method in [23] to a more general form, allowing us to obtain various discretization schemes by adjusting the value of θ. Additionally, by incorporating the concept of G-stability [25], we demonstrate the energy stability of the proposed uniform-time-step WSBDF2 method.

(ii) The other main contribution of this work is to design a new structure-preserving method by combining the variable-time-step WSBDF2 method with the SAV approach proposed in [46]. The adopted SAV approach differs from the traditional one [47], in order to construct the energy-stable algorithm based on variable-time-step method. By using different analytical technique as the uniform case, we also successfully obtain the mass conservation and energy stability of the constructed variable-time-step WSBDF2 method.

(iii) Furthermore, in order to eliminate the ill-posedness of the anisotropic model, it is indeed necessary to incorporate regularization terms in the continuous systems, especially for the strongly anisotropic case. The regularized models include the linear regularization and the Willmore regularization. In the process of practical computation, aiming to reduce the oscillations caused by the anisotropic surface energy function $\gamma(\cdot)$, we develop two stabilized methods for the uniform/variable-time-step WSBDF2 methods by adding two types of stabilization terms. The numerical experiments demonstrate that adding stabilization terms can maintain numerical stability without affecting the accuracy and structure-preservation of the solutions.

The rest of the paper is organized as follows. In Section 2, We provide a brief introduction to the anisotropic CH model and its regularized systems. In Section 3, two uniform-time-step numerical schemes are developed to the regularized systems, and their mass-conservation and energy-stability properties are rigorously proven. In Section 4, we develop two variable-time-step methods for solving the regularized systems, and also demonstrate their structure-preserving properties. Several numerical examples are given in section 5. Some conclusions follow in Section 6.

2. Anisotropic Cahn–Hilliard model equation and its energy law. In this section, we provide a brief introduction to the anisotropic CH model. Let $\Omega \in \mathbb{R}^d$ ($d = 2, 3$) be a smooth, open, bounded and connected domain, and let ϕ be an order parameter that takes values of ± 1 in the two phases with a smooth transition layer of thickness ϵ. The free energy density of Ginzburg-Landau-type is given by

$$(2.1) \qquad \mathcal{F}(\phi) = \gamma(\mathbf{n})\left(\frac{1}{2}|\nabla\phi|^2 + \frac{1}{\epsilon^2}F(\phi)\right),$$

where $\gamma(\mathbf{n})$ is a function describing the anisotropic property and $\mathbf{n}$ is the interface normal defined by

$$(2.2) \qquad \mathbf{n} = (n_1, n_2)^T = \frac{\nabla\phi}{|\nabla\phi|} \qquad or \qquad \mathbf{n} = (n_1, n_2, n_3)^T = \frac{\nabla\phi}{|\nabla\phi|},$$

and the energy density function takes the usual double-well form

$$(2.3) \qquad F(\phi) = \frac{1}{4}\left(\phi^2 - 1\right)^2.$$

Then, the surface free energy of the system is as follow

$$(2.4) \qquad \mathcal{E}(\phi) = \int_\Omega \mathcal{F}\,d\Omega.$$

The difference between isotropic system and anisotropic system lies in the choice of $\gamma(\mathbf{n})$. When $\gamma(\mathbf{n}) \equiv 1$, the system reflects isotropic properties. In the case of anisotropy, $\gamma(\mathbf{n})$ varies with $\mathbf{n}$ in a nontrivial way. In this paper, we consider the fourfold symmetric anisotropic function

$$(2.5) \qquad \gamma(\mathbf{n}) = 1 + \alpha\cos(4\vartheta) = 1 + \alpha\left(4\sum_{i=1}^{d} n_i^4 - 3\right),$$

where ϑ represents the orientation angle of the interfacial normal to the interface, and the non-negative parameter α in (2.5) describes the intensity of anisotropy. When $\alpha = 0$, an isotropic system is attained, namely, the free energy shows no preference for any orientations. When $\alpha \geq \frac{1}{15}$, the system becomes strongly anisotropic; i.e., the underlying Phase-filed equation is ill-posed. In order to regularize the original problem, an additional term $G(\phi)$, is introduced into (2.4) to penalize infinite curvatures in the resulting corners. As a result, the total system energy is modified as follow

$$(2.6) \qquad \mathcal{E}(\phi) = \int_\Omega\left(\mathcal{F} + \frac{\beta}{2}G\right)d\Omega,$$

where β is a regularization parameter. We consider two types of regularization with two distinct forms of G.

The first type is the linear regularization based on the bi-Laplacian of the phase variable

$$(2.7) \qquad G(\phi) = (\Delta\phi)^2,$$

and the second one is the nonlinear Willmore regularization with

$$(2.8) \qquad G(\phi) = \left(\Delta\phi - \frac{1}{\epsilon^2}f(\phi)\right)^2,$$

3

where $f(\phi) = F'(\phi) = \phi(\phi^2 - 1)$. By taking the H^{-1} gradient flow on the total system free energy (2.6), the anisotropic CH system with linear regularization is given by

$$\phi_t = \nabla \cdot (M(\phi)\nabla\mu), \tag{2.9a}$$

$$\mu = \frac{1}{\epsilon^2}\gamma(\mathbf{n})f(\phi) - \nabla \cdot \mathbf{m} + \beta\Delta^2\phi; \tag{2.9b}$$

and the system with Willmore regularization is represented by

$$\phi_t = \nabla \cdot (M(\phi)\nabla\mu), \tag{2.10a}$$

$$\mu = \frac{1}{\epsilon^2}\gamma(\mathbf{n})f(\phi) - \nabla \cdot \mathbf{m} + \beta\left(\Delta - \frac{1}{\epsilon^2}f'(\phi)\right)\left(\Delta\phi - \frac{1}{\epsilon^2}f(\phi)\right), \tag{2.10b}$$

where chemical potential μ is the variational derivative of $\mathcal{E}(\phi)$, $f'(\phi) = 3\phi^2 - 1$, $M(\phi) \geq M_0 > 0$ is the mobility function that depends on the phase variable ϕ or a constant, and the vector field $\mathbf{m}$ is given by

$$\mathbf{m} = \gamma(\mathbf{n})\nabla\phi + \frac{\mathbb{P}\nabla_{\mathbf{n}}\gamma(\mathbf{n})}{|\nabla\phi|}\left(\frac{1}{2}|\nabla\phi|^2 + \frac{1}{\epsilon^2}F(\phi)\right) \tag{2.11}$$

with $\mathbb{P} = \mathbb{I} - \mathbf{n}\mathbf{n}^T$. Without loss of generality, periodic boundary conditions are employed to eliminate the complexities associated with the boundary integrals. We also note that the boundary conditions can be of the no-flux type as

$$\left.\frac{\partial\phi}{\partial\mathbf{n}}\right|_{\partial\Omega} = \left.\frac{\partial\mu}{\partial\mathbf{n}}\right|_{\partial\Omega} = \left.\frac{\partial\omega}{\partial\mathbf{n}}\right|_{\partial\Omega} = 0, \tag{2.12}$$

where $\omega = \Delta\phi$ for the system with linear regularization and $\omega = \Delta\phi - \frac{1}{\epsilon^2}f(\phi)$ for the system with Willmore regularization .

For the linear regularization system, by taking the L^2 inner product of equation (2.9a) with $-\mu$ and equation (2.9b) with ϕ_t, employing integration by parts, and subsequently combining the two obtained equalities, one derives that the system (2.9) admits the following energy dissipative law

$$\frac{d}{dt}\mathcal{E}(\phi) = -\left\|\sqrt{M(\phi)}\nabla\mu\right\|^2 \leq 0, \tag{2.13}$$

where $\|\cdot\|$ is L^2-morm. Additionally, the CH model preserves local mass density. Indeed, by taking the L^2 inner product of equation (2.9a) with 1, the mass conservation property can be directly obtained using integration by parts, as follow

$$\frac{d}{dt}\int_\Omega \phi d\Omega = 0. \tag{2.14}$$

For the Willmore regularization system, the law of dissipation energy remains valid, while also conserving local mass density.

3. Numerical schemes on uniform temporal mesh. In this section, the schemes of uniform-time-step WSBDF2 method are built and studied. Let $\{t^n | t^n = n\tau, 0 \leq n \leq N\}$ be the time nodes on the interval $[0, T]$ with the uniform time step $\tau = T/N$, and denote u^n as the numerical solution of $u(t^n)$ for any function $u(t)$. Then, we define

$$D_\tau^\theta u^{n+\theta} = \frac{(\theta + \frac{1}{2})u^{n+1} - 2\theta u^n + (\theta - \frac{1}{2})u^{n-1}}{\tau}, \tag{3.1}$$

4

where $\theta \in [\frac{1}{2}, 1]$, and $D_\tau^\theta u^{n+\theta}$ is used to approximate the value of $u'(t^{n+\theta})$.

In order to prove the unconditional energy stability of subsequent numerical schemes, we initially introduce the concept of G-stability as described in the classic book by Hairer [25].

To simplify the presentation, we introduce a real, symmetric and positive definite matrix

$$G = \begin{pmatrix} g_{11} & g_{12} \\ g_{21} & g_{22} \end{pmatrix} = \begin{pmatrix} \frac{\theta(2\theta-1)}{2} & -\frac{(\theta+1)(2\theta-1)}{2} \\ -\frac{(\theta+1)(2\theta-1)}{2} & \frac{\theta(2\theta+3)}{2} \end{pmatrix},$$

and define the corresponding G-norm $\|\cdot\|_G$ with L^2 inner $(\cdot, \cdot)$ as follow

$$\|\mathbf{U}\|_G^2 = \sum_{i=1}^{2} \sum_{j=1}^{2} g_{i,j} \left(u^i, u^j \right), \tag{3.2}$$

where vector $\mathbf{U} = [u^1, u^2]^T$, with $u^1, u^2 \in L^2(\Omega)$. Clearly, if $\theta = \frac{1}{2}$, the G-norm will degenerate into the L^2-norm. When $\theta \in (\frac{1}{2}, 1]$, we can easily verify that the G-norm (3.2) is equivalent to the L^2-norm.

Similarly, we can define another G-norm $|\cdot|_G$ as

$$|\mathbf{V}|_G^2 = \sum_{i=1}^{2} \sum_{j=1}^{2} g_{i,j} v^i v^j \tag{3.3}$$

with vector $\mathbf{V} = [v^1, v^2]^T$, and $v^1, v^2 \in \mathbb{R}$.

After defining the G-norm $\|\cdot\|_G$ with L^2 inner $(\cdot, \cdot)$, we introduce the following lemma

LEMMA 3.1. *For any given sequence $\{u^n\}$, it holds*

$$\tau \left(D_\tau^\theta u^{n+\theta}, \theta u^{n+1} + (1-\theta)u^n \right) = \frac{\left\| \begin{bmatrix} u^{n+1} \\ u^n \end{bmatrix} \right\|_G^2 - \left\| \begin{bmatrix} u^n \\ u^{n-1} \end{bmatrix} \right\|_G^2}{2} + \frac{\left\| \alpha_2 u^{n+1} + \alpha_1 u^n + \alpha_0 u^{n-1} \right\|^2}{4}. \tag{3.4}$$

where $\alpha_0 = \alpha_2 = (\theta(2\theta - 1))^{\frac{1}{2}}$ and $\alpha_1 = -(\theta(2\theta - 1))^{\frac{1}{2}}$.

Proof. By the definitions of G-norm and simple algebraic operations, we can easily complete the proof. □

Similar to Lemma 3.1, for the G-norm $|\cdot|$, the following identity holds

$$\left(\frac{2\theta + 1}{2} v^{n+1} - 2\theta v^n + \frac{2\theta - 1}{2} v^{n-1} \right) \left(\theta v^{n+1} + (1-\theta)v^n \right)$$

$$= \frac{1}{2} \left\| \begin{bmatrix} v^{n+1} \\ v^n \end{bmatrix} \right\|_G^2 - \frac{1}{2} \left\| \begin{bmatrix} v^n \\ v^{n-1} \end{bmatrix} \right\|_G^2 + \frac{\left\| \alpha_2 v^{n+1} + \alpha_1 v^n + \alpha_0 v^{n-1} \right\|^2}{4}. \tag{3.5}$$

3.1. Linear regularization model. For the linear regularization system, we first introduce an auxiliary variable $r(t)$, defined by

$$r(t) = \sqrt{E_1(\phi)} := \sqrt{\int_\Omega \gamma(\mathbf{n}) \left(\frac{1}{2} |\nabla \phi|^2 + \frac{1}{\epsilon^2} F(\phi) \right) d\Omega + C},$$

where C is a positive constant that guarantees the radicand is positive. Then the total free energy (2.6) can be rewritten as

$$\mathcal{E}(r, \phi) = r^2 - C + \frac{\beta}{2} \int_\Omega (\Delta \phi)^2 d\Omega, \tag{3.6}$$

5

and the transformed H^{-1} gradient flow is given by

(3.7a)
$$\phi_t = \nabla \cdot (M(\phi)\nabla\mu),$$

(3.7b)
$$\mu = H(\phi)r + \beta\Delta^2\phi,$$

(3.7c)
$$r_t = \frac{1}{2}\int_\Omega H(\phi)\phi_t d\Omega,$$

where

(3.8)
$$H(\phi) = \frac{H_1(\phi)}{\sqrt{E_1(\phi)}} := \frac{\frac{1}{\epsilon^2}\gamma(\mathbf{n})f(\phi) - \nabla \cdot \mathbf{m}}{\sqrt{\int_\Omega \gamma(\mathbf{n})\left(\frac{1}{2}|\nabla\phi|^2 + \frac{1}{\epsilon^2}F(\phi)\right)d\Omega + C_0}}.$$

By taking the inner products of the above equations with μ, ϕ_t and $2r$, we can derive

(3.9)
$$\frac{d}{dt}\mathcal{E}(r,\phi) = -\left\|\sqrt{M(\phi)}\nabla\mu\right\|^2 \leq 0.$$

Namely, the transformed system (3.7) follows the new energy dissipation law.

We now construct a numerical scheme based on the uniform-time-step WSBDF2 method for the above system.

- **$\mathcal{U}_L$-method.** Given ϕ^n, r^n and ϕ^{n-1}, r^{n-1}, we update ϕ^{n+1}, r^{n+1} by solving

(3.10a) $D_\tau^\theta\phi^{n+\theta} = \nabla \cdot (M^{*,n+\theta}\nabla\mu^{n+\theta}),$

(3.10b) $\mu^{n+\theta} = H^{*,n+\theta}r^{n+\theta} + \beta\Delta^2\phi^{n+\theta} + \dfrac{S_1}{\epsilon^2}(\phi^{n+1} - 2\phi^n + \phi^{n-1}) - S_2\Delta(\phi^{n+1} - 2\phi^n + \phi^{n-1}),$

(3.10c) $D_\tau^\theta r^{n+\theta} = \dfrac{1}{2}\displaystyle\int_\Omega H^{*,n+\theta}D_\tau^\theta\phi^{n+\theta}d\Omega,$

where

$$\phi^{n+\theta} = \theta\phi^{n+1} + (1-\theta)\phi^n, \quad \phi^{*,n+\theta} = (1+\theta)\phi^n - \theta\phi^{n-1},$$
$$H^{*,n+\theta} = H(\phi^{*,n+\theta}), \quad M^{*,n+\theta} = M(\phi^{*,n+\theta}),$$

and S_i $(i = 1, 2)$ are positive stabilizing parameters.

REMARK 3.1. *In the above discretization scheme, we add two stabilization terms, $\frac{S_1}{\epsilon^2}(\phi^{n+1} - 2\phi^n + \phi^{n-1})$ and $S_2\Delta(\phi^{n+1} - 2\phi^n + \phi^{n-1})$, as they can eliminate the strong oscillations caused by $\gamma(\mathbf{n})$. These terms play a crucial role in maintaining the stability of the solution during computations. Additionally, $\frac{S_1}{\epsilon^2}(\phi^{n+1} - 2\phi^n + \phi^{n-1}) = \frac{S_1}{\epsilon^2}O(\tau^2)$ and $S_2\Delta(\phi^{n+1} - 2\phi^n + \phi^{n-1}) = S_2O(\tau^2)$, which mean they have second-order accuracy and thus do not affect the precision of the solution in practical calculations.* We can observe that solving a nonlocal and coupled system for ϕ^{n+1} and r^{n+1} within the framework of $\mathcal{U}_L$-method at each time step is a complex task. However, in practical applications, we can simplify the solving process by the following procedure.

We first rewrite (3.10c) as follow

$$r^{n+1} = \frac{1}{2}\int_\Omega H^{*,n+\theta}\phi^{n+1}d\Omega + \tilde{g}^n,$$

where

$$\tilde{g}^n = \frac{4\theta r^n - (2\theta - 1)r^{n-1}}{2\theta + 1} - \frac{1}{2}\int_\Omega H^{*,n+\theta}\frac{4\theta\phi^n - (2\theta - 1)\phi^{n-1}}{2\theta + 1}d\Omega.$$

Then the above equations can be written as

$$(3.11) \qquad A(\phi^{n+1}) - \frac{\theta}{2}\nabla \cdot (M^{*,n+\theta}\nabla(H^{*,n+\theta})) \int_{\Omega} H^{*,n+\theta}\phi^{n+1}d\Omega = g^n,$$

where

$$\begin{cases} A = \dfrac{2\theta+1}{2\tau}I - \nabla \cdot \left(M^{*,n+\theta}\nabla\left(\beta\theta\Delta^2 + S_1/\epsilon^2 I - S_2\Delta\right)\right), \\[2mm] g^n = \dfrac{4\theta\phi^n - (2\theta-1)\phi^{n-1}}{2\tau} + (\theta\tilde{g}^n + (1-\theta)r^n)\nabla \cdot (M^{*,n+\theta}\nabla(H^{*,n+\theta})) \\[2mm] \qquad - \nabla \cdot \left(M^{*,n+\theta}\nabla\left(\beta(1-\theta)\Delta^2\phi^n + S_1/\epsilon^2\phi^{*,n+1} - S_2\Delta\phi^{*,n+1}\right)\right). \end{cases}$$

By applying the linear operator A^{-1} to (3.11), then taking the L^2 inner product with $H^{*,n+\theta}$, we obtain

$$(3.12) \qquad \int_{\Omega} H^{*,n+\theta}\phi^{n+1}d\Omega = \frac{\int_{\Omega} H^{*,n+\theta}A^{-1}(g^n)d\Omega}{1 - \frac{\theta}{2}\int_{\Omega} H^{*,n+\theta}A^{-1}(\nabla \cdot (M^{*,n+\theta}\nabla(H^{*,n+\theta})))d\Omega}.$$

It is easy to verify the term $\int_{\Omega} H^{*,n+\theta}A^{-1}(\nabla \cdot (M^{*,n+\theta}\nabla(H^{*,n+\theta})))d\Omega \geq 0$ since $A^{-1}(\nabla \cdot (M^{*,n+\theta}\nabla(\cdot)))$ is a positive definite operator. Finally, we can solve ϕ^{n+1} from (3.11).

To sum up, the $\mathcal{U}_L$-method (3.10) can be easily implemented in the following steps:

- Compute $A^{-1}(g^n)$ and $A^{-1}(\nabla \cdot (M^{*,n+\theta}\nabla(H^{*,n+\theta})))$ by solving two sixth-order equations;

- Compute $\int_{\Omega} H^{*,n+\theta}\phi^{n+1}d\Omega$ from (3.12);

- Compute ϕ^{n+1} from the variation of (3.11) as follow

$$\phi^{n+1} = \frac{\theta}{2}A^{-1}(\nabla \cdot (M^{*,n+\theta}\nabla(H^{*,n+\theta}))) \int_{\Omega} H^{*,n+\theta}\phi^{n+1}d\Omega + A^{-1}(g^n).$$

Hence, the total cost at each time step essentially involves solving two fourth-order equations. Therefore, this method is extremely efficient and easy to implement.

Next, we give the proof that the $\mathcal{U}_L$-method (3.14) is unconditionally energy stable, and preserves mass conservation.

THEOREM 3.1. *The $\mathcal{U}_L$-method is unconditionally energy stable in the sense that*

$$(3.13) \qquad \frac{1}{\tau}(\mathcal{E}_L^{n+1} - \mathcal{E}_L^n) \leq - \left\| \sqrt{M^{*,n+\theta}}\nabla\mu^{n+\theta} \right\|^2 \leq 0,$$

where

$$(3.14) \qquad \mathcal{E}_L^{n+1} = \left\| \begin{bmatrix} r^{n+1} \\ r^n \end{bmatrix} \right\|_G^2 + \frac{\beta}{2}\left\| \begin{bmatrix} \Delta\phi^{n+1} \\ \Delta\phi^n \end{bmatrix} \right\|_G^2 + \frac{S_1}{\epsilon^2}\frac{\|\phi^{n+1} - \phi^n\|^2}{2} + S_2\frac{\|\nabla\phi^{n+1} - \nabla\phi^n\|^2}{2}.$$

Proof. Taking the L^2 inner product of (3.10a) with $\tau\mu^{n+\theta}$

$$(3.15) \qquad \left((\theta + \frac{1}{2})\phi^{n+1} - 2\theta\phi^n + (\theta - \frac{1}{2})\phi^{n-1}, \mu^{n+\theta}\right) = -\tau \left\| \sqrt{M^{*,n+\theta}}\nabla\mu^{n+\theta} \right\|^2.$$

By taking the L^2 inner product of (3.10b) with $(\theta + \frac{1}{2})\phi^{n+1} - 2\theta\phi^n + (\theta - \frac{1}{2})\phi^{n-1}$ and applying (3.4) along with the following identity:

$$(3.16) \quad ((2\theta+1)a - 4\theta b + (2\theta-1)c)(a - 2b + c) = (a - b)^2 - (b - c)^2 + 2\theta(a - 2b + c)^2,$$

7

we obtain

$$\left(\mu^{n+\theta}, (\theta + \frac{1}{2})\phi^{n+1} - 2\theta\phi^n + (\theta - \frac{1}{2})\phi^{n-1}\right)$$

$$= r^{n+\theta}\left(H^{*,n+\theta}, (\theta + \frac{1}{2})\phi^{n+1} - 2\theta\phi^n + (\theta - \frac{1}{2})\phi^{n-1}\right)$$

(3.17)
$$+ \beta\left(\frac{1}{2}\left\|\begin{bmatrix} \Delta\phi^{n+1} \\ \Delta\phi^n \end{bmatrix}\right\|_G^2 - \frac{1}{2}\left\|\begin{bmatrix} \Delta\phi^n \\ \Delta\phi^{n-1} \end{bmatrix}\right\|_G^2 + \frac{\left\|\alpha_2\Delta\phi^{n+1} + \alpha_1\Delta\phi^n + \alpha_0\Delta\phi^{n-1}\right\|^2}{4}\right)$$

$$+ \frac{S_1}{\epsilon^2}\left(\frac{\|\phi^{n+1} - \phi^n\|^2}{2} - \frac{\|\phi^n - \phi^{n-1}\|^2}{2} + \theta\|\phi^{n+1} - 2\phi^n + \phi^{n-1}\|^2\right)$$

$$+ S_2\left(\frac{\|\nabla\phi^{n+1} - \nabla\phi^n\|^2}{2} - \frac{\|\nabla\phi^n - \nabla\phi^{n-1}\|^2}{2} + \theta\|\nabla\phi^{n+1} - 2\nabla\phi^n + \nabla\phi^{n-1}\|^2\right).$$

By multiplying (3.10c) with $r^{n+\theta}$ and using (3.5), we have

(3.18)
$$\frac{1}{2}\left\|\begin{bmatrix} r^{n+1} \\ r^n \end{bmatrix}\right\|_G^2 - \frac{1}{2}\left\|\begin{bmatrix} r^n \\ r^{n-1} \end{bmatrix}\right\|_G^2 + \frac{\left|\alpha_2 r^{n+1} + \alpha_1 r^n + \alpha_0 r^{n-1}\right|^2}{4}$$

$$= \frac{1}{2}r^{n+\theta}\int_\Omega H^{*,n+\theta}\left((\theta + \frac{1}{2})\phi^{n+1} - 2\theta\phi^n + (\theta - \frac{1}{2})\phi^{n-1}\right)d\Omega.$$

Combining the equations (3.15),(3.17) and (3.18), we derive

$$\left\|\begin{bmatrix} r^{n+1} \\ r^n \end{bmatrix}\right\|_G^2 - \left\|\begin{bmatrix} r^n \\ r^{n-1} \end{bmatrix}\right\|_G^2 + \frac{\beta}{2}\left(\left\|\begin{bmatrix} \Delta\phi^{n+1} \\ \Delta\phi^n \end{bmatrix}\right\|_G^2 - \left\|\begin{bmatrix} \Delta\phi^n \\ \Delta\phi^{n-1} \end{bmatrix}\right\|_G^2\right)$$

$$+ \frac{S_1}{\epsilon^2}\left(\frac{\|\phi^{n+1} - \phi^n\|^2}{2} - \frac{\|\phi^n - \phi^{n-1}\|^2}{2}\right) + S_2\left(\frac{\|\nabla\phi^{n+1} - \nabla\phi^n\|^2}{2} - \frac{\|\nabla\phi^n - \nabla\phi^{n-1}\|^2}{2}\right)$$

(3.19)
$$+ \frac{\left|\alpha_2 r^{n+1} + \alpha_1 r^n + \alpha_0 r^{n-1}\right|^2}{2} + \frac{\beta}{2}\left(\frac{\left\|\alpha_2\Delta\phi^{n+1} + \alpha_1\Delta\phi^n + \alpha_0\Delta\phi^{n-1}\right\|^2}{2}\right)$$

$$+ \frac{\theta S_1}{\epsilon^2}\|\phi^{n+1} - 2\phi^n + \phi^{n-1}\|^2 + \theta S_2|\nabla\phi^{n+1} - 2\nabla\phi^n + \nabla\phi^{n-1}\|^2$$

$$= -\tau\|\sqrt{M^{*,n+\theta}}\nabla\mu^{n+\theta}\|^2.$$

Finally, we obtain the desired result by omitting the positive terms. $\square$

THEOREM 3.2. *The solution of the $\mathcal{U}_L$-method* (3.10) *satisfies the mass conservation.*

Proof. By taking the inner product of equation (3.10a) with 1, we can immediately obtain

$$\left(\frac{(\theta + \frac{1}{2})u^{n+1} - 2\theta u^n + (\theta - \frac{1}{2})u^{n-1}}{\tau}, 1\right) = \nabla \cdot (M^{*,n+\theta}\nabla\mu^{n+\theta}) = 0,$$

namely

$$\int_\Omega \phi^{n+1}d\Omega = \frac{4\theta}{2\theta + 1}\int_\Omega \phi^n d\Omega - \frac{2\theta - 1}{2\theta + 1}\int_\Omega \phi^{n-1}d\Omega.$$

By applying mathematical induction with the initial condition $\int_\Omega \phi^1 d\Omega = \int_\Omega \phi^0 d\Omega$, we can conclude

(3.20)
$$\int_\Omega \phi^{n+1}d\Omega = \int_\Omega \phi^n d\Omega = \cdots = \int_\Omega \phi^1 d\Omega = \int_\Omega \phi^0 d\Omega.$$

8

The proof is complete. □

REMARK 3.2. *Since the BDF2 method is a two-step method, we use the BDF1 method, also known as the backward Euler method, to compute ϕ^1. For this method, we can easily obtain that $\int_\Omega \phi^1 d\Omega = \int_\Omega \phi^0 d\Omega$, which means that mass conservation is maintained in the first step of the computation.*

3.2. Willmore regularization model. we consider the Willmore regularization model in this subsection. Similar to the case of linear regularization model, we define an auxiliary variable as follow

$$r(t) = \sqrt{E_2(\phi)} := \sqrt{\int_\Omega \left[\gamma(\mathbf{n}) \left(\frac{1}{2}|\nabla\phi|^2 + \frac{1}{\epsilon^2}F(\phi) \right) + \frac{\beta}{2} \left(\Delta\phi - \frac{1}{\epsilon^2}f(\phi) \right)^2 \right] d\Omega + C},$$

where C is a positive constant that ensures the radicand is positive. Then the total free energy can (2.6) be rewritten as

$$(3.21) \qquad\qquad \mathcal{E}(r, \phi) = r^2 - C,$$

and the transformed H^{-1} gradient flow is given by

$$(3.22a) \qquad\qquad \phi_t = \nabla \cdot (M(\phi)\nabla\mu),$$

$$(3.22b) \qquad\qquad \mu = Z(\phi)r,$$

$$(3.22c) \qquad\qquad r_t = \frac{1}{2} \int_\Omega Z(\phi)\phi_t d\Omega,$$

where

$$(3.23) \quad Z(\phi) = \frac{Z_1(\phi)}{\sqrt{E_2(\phi)}} := \frac{\frac{1}{\epsilon^2}\gamma(\mathbf{n})f(\phi) - \nabla \cdot \mathbf{m} + \beta \left(\Delta\phi - \frac{1}{\epsilon}f(\phi) \right) \left(\Delta\phi - \frac{1}{\epsilon^2}f'(\phi) \right)}{\sqrt{\int_\Omega \left(\gamma(\mathbf{n}) \left(\frac{1}{2}|\nabla\phi|^2 + \frac{1}{\epsilon}F(\phi) \right) + \frac{\beta}{2} \left(\Delta\phi - \frac{1}{\epsilon}f(\phi) \right)^2 \right) d\Omega + C}}.$$

Similar as the linear regularization model, by taking the inner products of the above equations with μ, ϕ_t and $2r$, we can derive

$$(3.24) \qquad\qquad \frac{d}{dt}\mathcal{E}(r, \phi) = -\left\| \sqrt{M(\phi)}\nabla\mu \right\|^2 \leq 0.$$

Namely, the transformed linear regularization system (3.22) follows the modified energy dissipation law.

We now construct a numerical scheme based on the uniform-time-step WSBDF2 method for the system (3.22).

- $\mathcal{U}_W$-**method.** Given ϕ^n, r^n and ϕ^{n-1}, r^{n-1}, we update ϕ^{n+1}, r^{n+1} by solving

$$(3.25a) \qquad D_\tau^\theta \phi^{n+\theta} = \nabla \cdot (M^{*,n+\theta}\nabla\mu^{n+\theta}),$$

$$(3.25b) \qquad \begin{aligned} \mu^{n+\theta} &= Z^{*,n+\theta}r^{n+\theta} + \frac{S_1}{\epsilon^2}(\phi^{n+1} - 2\phi^n + \phi^{n-1}) \\ &\quad - S_2\Delta(\phi^{n+1} - 2\phi^n + \phi^{n-1}) + S_3\Delta^2(\phi^{n+1} - 2\phi^n + \phi^{n-1}), \end{aligned}$$

$$(3.25c) \qquad D_\tau^\theta r^{n+\theta} = \frac{1}{2} \int_\Omega Z^{*,n+\theta}D_\tau^\theta \phi^{n+\theta} d\Omega,$$

where $Z^{*,n+\theta} = Z(\phi^{*,n+\theta})$ and S_i $(i = 1, 2, 3)$ are positive stabilizing parameters.

9

The following two theorems demonstrate that the structure-preserving properties still hold for the Willmore regularization system. Additionally, since the proof processes are similar to Theorem 3.1 and Theorem 3.2, the proofs are omitted here.

THEOREM 3.3. *The $\mathcal{U}_W$-method is unconditionally energy stable in the sense that*

$$(3.26) \qquad \frac{1}{\tau}(\mathcal{E}_W^{n+1} - \mathcal{E}_W^n) \leq - \left\| \sqrt{M^{*,n+\theta}}\nabla\mu^{n+\theta} \right\|^2 \leq 0,$$

where

$$(3.27) \quad \mathcal{E}_W^{n+1} = \left\| \begin{bmatrix} r^{n+1} \\ r^n \end{bmatrix} \right\|_G^2 + \frac{S_1}{\epsilon^2} \frac{\|\phi^{n+1} - \phi^n\|^2}{2} + S_2\frac{\|\nabla\phi^{n+1} - \nabla\phi^n\|^2}{2} + S_3\frac{\|\Delta\phi^{n+1} - \Delta\phi^n\|^2}{2}.$$

THEOREM 3.4. *The solution of the $\mathcal{U}_W$-method (3.25) satisfies the mass conservation.*

4. Numerical scheme on nonuniform temporal mesh. In this section, we introduce the varia-time-step WSBDF2 method for the anisotropic model and prove its property of energy stability.

Choose the time levels $0 = t_0 < t_1 < t_2 < \cdots < t_N = T$ with the $\tau_n := t_n - t_{n-1}$ for $1 \leq n \leq N$. Let $\gamma_{n+1} = \tau_{n+1}/\tau_n$ be the adjacent time step ratios and set $\tau = max\{\tau_n, 1 \leq n \leq N\}$ as the maximum time step size. For any sequence $\{u^n\}_{n=0}^N$, we denote $\nabla_\tau u^n := u^n - u^{n-1}$ for $1 \leq n \leq N$ and define

$$(4.1) \qquad \tilde{D}_\tau^\theta u^{n+\theta} = \frac{1 + 2\theta\gamma_{n+1}}{\tau_{n+1}(1 + \gamma_{n+1})}\nabla_\tau u^{n+1} + \frac{(1 - 2\theta)\gamma_{n+1}^2}{\tau_{n+1}(1 + \gamma_{n+1})}\nabla_\tau u^n.$$

However, unfortunately, on the nonuniform temporal mesh, we cannot derive a result similar to Lemma 3.1. This is because, if we follow the approach similar to that used to introduce the G-norm for achieving (3.4), inspired by the uniform G-stability idea, we cannot obtain a real, symmetric, and positive definite matrix, and thus we do not achieve energy dissipation.

In order to prove unconditional energy stability on nonuniform temporal mesh, we need to introduce the Theorem 3.1 in [40] or Lemma 2.1 in [48].

LEMMA 4.1. *Let the adjacent step ratios γ_{n+1} satisfy $0 \leq \gamma_{n+1} \leq \gamma_*$, then it holds that*

$$(4.2) \qquad \tilde{D}_2^{n+\theta}\phi^{n+\theta}(\phi^{n+1} - \phi^n) \geq R_\theta^{n+1} - R_\theta^n + R(\gamma_{n+1}, \gamma_{n+2})\frac{\|\phi^{n+1} - \phi^n\|^2}{2\tau_{n+1}},$$

where γ_* is the positive root of equation

$$(1 - 2\theta)^2\gamma_*^3 - 4\theta^2\gamma_*^2 - 4\theta\gamma_* - 1 = 0,$$

and

$$R_\theta^n = \frac{(2\theta - 1)\gamma_{n+1}^{3/2}}{2(1 + \gamma_{n+1})}\frac{\|\phi^n - \phi^{n-1}\|^2}{\tau_n}, \quad R(x,y) := \frac{2(1 + 2\theta x) + (1 - 2\theta)x^{3/2}}{1 + x} - \frac{(2\theta - 1)y^{3/2}}{1 + y}.$$

It is easy to verify that $R(x, y)$ is increasing in interval $(0, 1)$ and decreasing in the interval with respect to x. Additionally, $R(x, y)$ is decreasing with respect to y. Then we have

$$R(x, y) \geq min\{R(0, \gamma_*), R(\gamma_*, \gamma_*)\} = \frac{(1 - 2\theta)^2\gamma_*^3 - 4\theta^2\gamma_*^2 - 4\theta\gamma_* - 1}{1 + \gamma_*} = 0, \quad 0 \leq x, y \leq \gamma_*.$$

Moreover, we can easily check that the root γ_* is decreasing for $\theta \in [\frac{1}{2}, 1]$. In particular, $\gamma_* = 4.8645365123$ if $\theta = 1$ and $\gamma_* \to \infty$ if $\theta = \frac{1}{2}$.

4.1. Linear regularization model. Different from the SAV approach on uniform temporal mesh, we reintroduce an auxiliary variable, denoted by

$$u(t) = \sqrt{\widetilde{E}_1(\phi)} := \sqrt{\int_\Omega \gamma(\mathbf{n})\left(\frac{1}{2}|\nabla\phi|^2 + \frac{1}{\epsilon^2}F(\phi)\right) - \frac{\lambda_1}{2\epsilon^2}|\phi|^2 - \frac{\lambda_2}{2}|\nabla\phi|^2 \, d\Omega + C_0},$$

where C_0 is a positive constant selected to ensure the value $\widetilde{E}_1$ is positive. Now, the total free energy (2.6) can be rewritten as

$$(4.3) \qquad \mathcal{E}(u,\phi) = u^2 + \frac{\beta}{2}\int_\Omega (\Delta\phi)^2 d\Omega + \int_\Omega \left(\frac{\lambda_1}{2\epsilon^2}|\phi|^2 + \frac{\lambda_2}{2}|\nabla\phi|^2\right)d\Omega - C_0.$$

Then, we can obtain a modified gradient flow

$$(4.4\text{a}) \qquad \phi_t = \nabla \cdot (M(\phi)\nabla\mu),$$

$$(4.4\text{b}) \qquad \mu = \frac{u}{\sqrt{\widetilde{E}_1(\phi)}}V(\xi)\mathcal{H}(\phi) + \beta\Delta^2\phi + \frac{\lambda_1}{\epsilon^2}\phi - \lambda_2\Delta\phi,$$

$$(4.4\text{c}) \qquad u_t = \frac{V(\xi)}{2\sqrt{\widetilde{E}_1(\phi)}}\int_\Omega \mathcal{H}(\phi)\phi_t d\Omega,$$

where

$$(4.5) \qquad \mathcal{H}(\phi) = \frac{1}{\epsilon^2}\gamma(\mathbf{n})f(\phi) - \nabla \cdot \mathbf{m} - \frac{\lambda_1}{\epsilon^2}\phi + \lambda_2\Delta\phi,$$

and $V(\xi) \in C^2(\mathbb{R})$ is a real positive function with $V(1) \equiv 1$. Taking L^2 inner product of equations in (4.4) with μ, ϕ_t and $2u$ respectively, we can obtain

$$(4.6) \qquad \frac{d}{dt}\mathcal{E}(u,\phi) = -\left\|\sqrt{M(\phi)}\nabla\mu\right\|^2 \le 0,$$

which means that the modified system (4.4) satisfies the unconditional energy stability.

In what follows, we construct a numerical scheme with variable-time-step method to discretize the above linear regularized system.

- $\mathcal{V}_L$**-method.** Given ϕ^n, r^n and ϕ^{n-1}, update ϕ^{n+1}, r^{n+1} by solving

$$(4.7\text{a}) \qquad \tilde{D}_2^{n+\theta}\phi^{n+\theta} = \nabla \cdot (M^{*,n+\theta}\nabla\mu^{n+\theta}),$$

$$(4.7\text{b}) \qquad \mu^{n+\theta} = \frac{u^{n+1}}{\sqrt{\widetilde{E}_1^n}}V(\xi^{n+1})\mathcal{H}^{*,n+\theta} + \beta\Delta^2\phi^{n+\theta} + \frac{\lambda_1}{\epsilon^2}\phi^{n+\theta} - \lambda_2\Delta\phi^{n+\theta},$$

$$(4.7\text{c}) \qquad \frac{u^{n+1} - u^n}{\tau_{n+1}} = \frac{V(\xi^{n+1})}{2\sqrt{\widetilde{E}_1^n}}\int_\Omega \mathcal{H}^{*,n+\theta}\frac{\phi^{n+1} - \phi^n}{\tau_{n+1}}d\Omega,$$

where

$$\xi^{n+1} = \frac{u^{n+1}}{\sqrt{\widetilde{E}_1^n}}, \quad \phi^{n+\theta} = \theta\phi^{n+1} + (1-\theta)\phi^n, \quad \phi^{*,n+\theta} = (1+\theta\gamma_{n+1})\phi^n - \theta\gamma_{n+1}\phi^{n-1},$$

11

λ_i (i=1,2) are positive constants and $\lim\limits_{\xi\to 1}\frac{V(\xi)-1}{1-\xi} = 1$ with $V(1) = 1$. Considering (4.7c), it is clear that the numerical approximations for u^{n+1} is a first-order approximation of $u(t)$, and thus, ξ^{n+1} have only first-order accuracy of 1 in time, which means that

(4.8) $$u^{n+1} = u(t^{n+1}) + O(\tau_{n+1}), \quad \xi^{n+1} = 1 + O(\tau_{n+1}).$$

Therefore, it may initially appear that the scheme we construct is first-order accuracy, but in reality, the phase function ϕ in the original gradient flow (2.9) is not directly influenced by $r(t)$ and ξ; instead, it is controlled by $\frac{u(t)}{\sqrt{\widetilde{E}_1}}V(\xi)$. Hence, the scheme we develop is, in fact, second-order accuracy. Due to the limitations in the length of this paper, we plan to conduct an error analysis of this scheme in our future work.

Next, we will show how to efficiently solve the $\mathcal{U}_L$-method (4.7). It follows from (4.7a) that

(4.9) $$A(\phi^{n+1}) - \xi^{n+1}V(\xi^{n+1})\nabla\cdot(M^{*,n+\theta}\nabla(\mathcal{H}^{*,n+\theta})) = g^n,$$

where

$$
\begin{cases}
A = \dfrac{1 + 2\theta\gamma_{n+1}}{\tau_{n+1}(1 + \gamma_{n+1})}I - \theta\nabla\cdot\left(M^{*,n+\theta}\nabla\left(\beta\Delta^2 + \dfrac{\lambda_1}{\epsilon^2}I - \lambda_2\Delta\right)\right), \\[4mm]
g^n = \dfrac{1}{\tau_{n+1}}\left((1 + (2\theta - 1)\gamma_{n+1})\phi^n - \dfrac{(2\theta - 1)\gamma_{n+1}^2}{1 + \gamma_{n+1}}\phi^{n-1}\right) \\[4mm]
\qquad + (1 - \theta)\nabla\cdot\left(M^{*,n+\theta}\nabla\left(\beta\Delta^2 + \dfrac{\lambda_1}{\epsilon^2}I - \lambda_2\Delta\right)\right).
\end{cases}
$$

Then we denote

(4.10) $$\phi^{n+1} = \phi_1^{n+1} + \xi^{n+1}V(\xi^{n+1})\phi_2^{n+1}$$

with ϕ_1^{n+1} and ϕ_2^{n+1} being solved respectively by

(4.11) $$A(\phi_1^{n+1}) = g^n, \quad A(\phi_2^{n+1}) = \nabla\cdot(M^{*,n+\theta}\nabla(\mathcal{H}^{*,n+\theta})).$$

Next, we numerically solve for ξ^{n+1} by substituting (4.10) into (4.7c), resulting in

(4.12) $$\xi^{n+1}\sqrt{\widetilde{E}_1^n} - u^n - \frac{V(\xi^{n+1})}{2\sqrt{\widetilde{E}_1^n}}\left[\xi^{n+1}V(\xi^{n+1})\left(\mathcal{H}^{*,n+\theta},\phi_2^{n+1}\right) + \left(\mathcal{H}^{*,n+\theta},\phi_1^{n+1} - \phi^n\right)\right] = 0.$$

Denoting the left side of the above equation by $W(\xi^{n+1})$, combining $V(1) = 1$ and the turth $V'(1) = -1$, we obtain the following identities

(4.13)
$$W(1) = \sqrt{\widetilde{E}_1^n} - u^n - \frac{\left(\mathcal{H}^{*,n+\theta},\phi_1^{n+1} + \phi_2^{n+1} - \phi^n\right)}{2\sqrt{\widetilde{E}_1^n}} \sim O(\tau_{n+1}),$$

$$W'(1) = \sqrt{\widetilde{E}_1^n} + \frac{\left(\mathcal{H}^{*,n+\theta},\phi_1^{n+1} + \phi_2^{n+1} - \phi^n\right)}{2\sqrt{\widetilde{E}_1^n}} \sim \sqrt{\widetilde{E}_1^n} + O(\tau_{n+1}).$$

Therefore, ξ^{n+1} can be efficiently computed by solving the nonlinear algebraic equation (4.12) using Newton's iteration, starting with $\xi^0 = 1$ and a sufficiently large C, since we only require first-order accuracy for ξ^{n+1} in time within the $\mathcal{V}_L$-method (4.7). To sum up, the $\mathcal{V}_L$-method (4.7) can be easily implemented in the following steps:

- Compute ϕ_1^{n+1} and ϕ_2^{n+1} form (4.11);
- Compute ξ^{n+1} from (4.12), and then ϕ^{n+1} can be obtain by using (4.10).

Hence, this method is extremely efficient and easy to implement.

Then, we give the proof that the $\mathcal{V}_L$-method (4.15) is unconditionally energy stable, and preserves mass conservation

THEOREM 4.1. *For $\theta \in [\frac{1}{2}, 1]$ and $0 \le \gamma_{n+1} \le \gamma_*$, with $M(\phi)$ in (2.9) is a positive constant or a time-dependent positive function, the $\mathcal{V}_L$-method is unconditionally energy stable in the sense that*

(4.14) $$\tilde{\mathcal{E}}_L^{n+1} - \tilde{\mathcal{E}}_L^n \le 0,$$

where the modified energy is defined by

(4.15)
$$\tilde{\mathcal{E}}_L^{n+1} = \frac{(2\theta - 1)\gamma_{n+2}^{3/2}}{2(1 + \gamma_{n+2})} \frac{\|\nabla^{-1}(\phi^{n+1} - \phi^n)\|^2}{M\tau_{n+1}} + \frac{\beta}{2}\|\Delta\phi^{n+1}\|^2$$
$$+ \frac{\lambda_1}{2\epsilon^2}\|\phi^{n+1}\|^2 + \frac{\lambda_2}{2}\|\nabla\phi^{n+1}\|^2 + |u^{n+1}|^2.$$

Proof. Setting $M^{*,n+\theta} = M$ in (4.7a) and taking the inner products of (4.7a) and (4.7b) with $-\frac{1}{M}\Delta^{-1}(\phi^{n+1} - \phi^n)$ and $\phi^{n+1} - \phi^n$ respectively

(4.16) $$\left(\tilde{D}_2^{n+\theta}\phi^{n+\theta}, -\frac{1}{M}\Delta^{-1}(\phi^{n+1} - \phi^n)\right) = -\left(\mu^{n+\theta}, \phi^{n+1} - \phi^n\right),$$

and

(4.17)
$$\left(\mu^{n+\theta}, \phi^{n+1} - \phi^n\right) = \frac{u^{n+1}}{\sqrt{\tilde{E}_1^n}} V(\xi^{n+1}) \left(\mathcal{H}^{*,n+\theta}, \phi^{n+1} - \phi^n\right) + \beta\left(\Delta^2\phi^{n+\theta}, \phi^{n+1} - \phi^n\right)$$
$$+ \frac{\lambda_1}{\epsilon^2}\left(\phi^{n+\theta}, \phi^{n+1} - \phi^n\right) - \lambda_2\left(\Delta\phi^{n+\theta}, \phi^{n+1} - \phi^n\right).$$

Then, by multiplying (4.7c) with $2u^{n+1}$, we obtain

(4.18) $$\frac{2u^{n+1}(u^{n+1} - u^n)}{\tau_{n+1}} = \frac{u^{n+1}V(\xi^{n+1})}{\sqrt{\tilde{E}_1^n}} \int_\Omega \mathcal{H}^{*,n+\theta} \frac{\phi^{n+1} - \phi^n}{\tau_{n+1}} d\Omega.$$

It follows from the above equations that

(4.19)
$$\left(\tilde{D}_2^{n+\theta}\phi^{n+\theta}, -\frac{1}{M}\Delta^{-1}(\phi^{n+1} - \phi^n)\right) + \beta\left(\Delta^2\phi^{n+\theta}, \phi^{n+1} - \phi^n\right) + 2u^{n+1}(u^{n+1} - u^n)$$
$$+ \frac{\lambda_1}{\epsilon^2}\left(\phi^{n+\theta}, \phi^{n+1} - \phi^n\right) + \lambda_2\left(\nabla\phi^{n+\theta}, \nabla(\phi^{n+1} - \phi^n)\right) = 0.$$

By applying the inequality (4.2) and the identities

(4.20a) $$2\left(\theta a^{k+1} + (1 - \theta)a^k\right)\left(a^{k+1} - a^k\right) = |a^{k+1}|^2 - |a^k|^2 + (2\theta - 1)|a^{k+1} - a^k|^2,$$

(4.20b) $$2a^{k+1}\left(a^{k+1} - a^k\right) = |a^{k+1}|^2 - |a^k|^2 + |a^{k+1} - a^k|^2,$$

13

we have

$$(4.21)$$

$$\frac{(2\theta-1)\gamma_{n+2}^{3/2}}{2(1+\gamma_{n+2})}\frac{\|\nabla^{-1}\phi^{n+1}-\nabla^{-1}\phi^{n}\|^{2}}{M\tau_{n+1}} - \frac{(2\theta-1)\gamma_{n+1}^{3/2}}{2(1+\gamma_{n+1})}\frac{\|\nabla^{-1}\phi^{n}-\nabla^{-1}\phi^{n-1}\|^{2}}{M\tau_{n}} + \frac{\beta}{2}\|\Delta\phi^{n+1}\|^{2}$$

$$-\frac{\beta}{2}\|\Delta\phi^{n}\|^{2} + \frac{\lambda_{1}}{2\epsilon^{2}}\|\phi^{n+1}\|^{2} - \frac{\lambda_{1}}{2\epsilon^{2}}\|\phi^{n}\|^{2} + \frac{\lambda_{2}}{2}\|\nabla\phi^{n+1}\|^{2} - \frac{\lambda_{2}}{2}\|\nabla\phi^{n}\|^{2}$$

$$+|u^{n+1}|^{2} - |u^{n}|^{2} + R(\gamma_{n+1},\gamma_{n+2})\frac{\|\phi^{n+1}-\phi^{n}\|^{2}}{2M\tau_{n+1}} + \frac{\beta(2\theta-1)}{2}\|\Delta\phi^{k}-\Delta\phi^{k-1}\|^{2}$$

$$+\frac{\lambda_{1}(2\theta-1)}{2\epsilon^{2}}\|\phi^{k}-\phi^{k-1}\|^{2} + \frac{\lambda_{2}(2\theta-1)}{2}\|\nabla\phi^{k}-\nabla\phi^{k-1}\|^{2} + |u^{k+1}-u^{k}|^{2} \le 0.$$

Finally, we obtain the desired result by omitting the positive terms. □

THEOREM 4.2. *The solution of the $\mathcal{V}_{L}$-method (4.7) satisfies the mass conservation.*

Proof. By taking the inner product of equation (4.7a) with 1, we can immediately obtain

$$\left(\frac{1+2\theta\gamma_{n+1}}{\tau_{n+1}(1+\gamma_{n+1})}\nabla_{\tau}\phi^{n+1} + \frac{(1-2\theta)\gamma_{n+1}^{2}}{\tau_{n+1}(1+\gamma_{n+1})}\nabla_{\tau}\phi^{n}, 1\right) = \nabla\cdot(M^{*,n+\theta}\nabla\mu^{n+\theta}) = 0,$$

namely

$$\int_{\Omega}\phi^{n+1}d\Omega = \left(1 - \frac{(1-2\theta)\gamma_{n}^{2}}{1+2\theta\gamma_{n}}\right)\int_{\Omega}\phi^{n}d\Omega - \frac{(1-2\theta)\gamma_{n}^{2}}{1+2\theta\gamma_{n}}\int_{\Omega}\phi^{n-1}d\Omega.$$

By applying mathematical induction with the initial condition $\int_{\Omega}\phi^{1}d\Omega = \int_{\Omega}\phi^{0}d\Omega$, we can conclude

$$(4.22) \qquad \int_{\Omega}\phi^{n+1}d\Omega = \int_{\Omega}\phi^{n}d\Omega = \cdots = \int_{\Omega}\phi^{1}d\Omega = \int_{\Omega}\phi^{0}d\Omega.$$

The proof is complete. □

4.2. Willmore regularization model. For the Willmore regularization model on the nonuniform temporal mesh, we need to redefine the auxiliary variable $u(t)$ as follows

$$u(t) = \sqrt{\widetilde{E}_{2}(\phi)} := \sqrt{\int_{\Omega}\left(g(\phi) - \frac{\lambda_{1}}{2\epsilon^{2}}|\phi|^{2} - \frac{\lambda_{2}}{2}|\nabla\phi|^{2} - \frac{\lambda_{3}}{2}|\Delta\phi|^{2}\right)d\Omega + C_{0}},$$

where C_{0} is a positive constant to ensure $\widetilde{E}_{2}(\phi) > 0$ and

$$g(\phi) = \gamma(\mathbf{n})\left(\frac{1}{2}|\nabla\phi|^{2} + \frac{1}{\epsilon^{2}}F(\phi)\right) + \frac{\beta}{2}\left(\Delta\phi - \frac{1}{\epsilon^{2}}f(\phi)\right)^{2}.$$

Thus, a new modified energy for the Willmore regularization model can be given by

$$(4.23) \qquad \mathcal{E}(u,\phi) = u^{2} + \int_{\Omega}\left(\frac{\lambda_{1}}{2\epsilon^{2}}|\phi|^{2} + \frac{\lambda_{2}}{2}|\nabla\phi|^{2} + \frac{\lambda_{3}}{2}|\Delta\phi|^{2}\right)d\Omega - C_{0}.$$

Then, we can obtain the corresponding gradient flow

$$(4.24a) \qquad \phi_{t} = \nabla\cdot(M(\phi)\nabla\mu),$$

$$(4.24b) \qquad \mu = \frac{u}{\sqrt{\widetilde{E}_{2}(\phi)}}V(\xi)\mathcal{Z}(\phi) + \frac{\lambda_{1}}{\epsilon^{2}}\phi - \lambda_{2}\Delta\phi + \lambda_{3}\Delta^{2}\phi,$$

$$(4.24c) \qquad u_{t} = \frac{V(\xi)}{2\sqrt{\widetilde{E}_{2}(\phi)}}\int_{\Omega}\mathcal{Z}(\phi)\phi_{t}d\Omega,$$

14

where

(4.25)

$$\mathcal{Z}(\phi) = \frac{1}{\epsilon^2}\gamma(\mathbf{n})f(\phi) - \nabla \cdot \mathbf{m} + \beta\left(\Delta\phi - \frac{1}{\epsilon^2}f(\phi)\right)\left(\Delta\phi - \frac{1}{\epsilon^2}f'(\phi)\right) - \frac{\lambda_1}{\epsilon^2}\phi + \lambda_2\Delta\phi - \lambda_3\Delta^2\phi,$$

and $V(\xi) \in C^2(\mathbb{R})$ is a real function. Taking L^2 inner product of equations in (4.24) with μ, ϕ_t and $2u$ respectively, we can obtain

(4.26)
$$\frac{d}{dt}\mathcal{E}(u,\phi) = -\left\|\sqrt{M(\phi)}\nabla\mu\right\|^2 \le 0.$$

Then, we discretize the above modified model(4.24) using the variable-time-step WSBDF2 method.

- $\mathcal{V}_W$-**method.** Given ϕ^n, u^n and ϕ^{n-1}, update ϕ^{n+1}, u^{n+1} by solving

(4.27a)
$$\tilde{D}_2^{n+\theta}\phi^{n+\theta} = \nabla \cdot (M^{*,n+\theta}\nabla\mu^{n+\theta}),$$

(4.27b)
$$\mu^{n+\theta} = \frac{u^{n+1}}{\sqrt{\widetilde{E}_2^n}}V(\xi^{n+1})\mathcal{Z}^{*,n+\theta} + \frac{S_1}{\epsilon^2}\phi^{n+\theta} - S_2\Delta\phi^{n+\theta} + S_3\Delta^2\phi^{n+\theta},$$

(4.27c)
$$\frac{u^{n+1} - u^n}{\tau_{n+1}} = \frac{V(\xi^{n+1})}{2\sqrt{\widetilde{E}_2^n}}\int_\Omega \mathcal{Z}^{*,n+\theta}\frac{\phi^{n+1} - \phi^n}{\tau_{n+1}}d\Omega.$$

The following two theorems demonstrate that the structure-preserving properties still hold for the Willmore regularization system. Additionally, since the proof processes are similar to Theorem 4.1 and Theorem 4.2, the proofs are omitted here.

THEOREM 4.3. *For $\theta \in [\frac{1}{2}, 1]$ and $0 \le \gamma_{n+1} \le \gamma_*$, if $M(\phi)$ in (2.10) is a positive constant, the $\mathcal{V}_W$-method is unconditionally energy stable in the sense that*

(4.28)
$$\tilde{\mathcal{E}}_W^{n+1} - \tilde{\mathcal{E}}_W^n \le 0,$$

where the modified energy is defined by

(4.29)
$$\tilde{\mathcal{E}}_W^{n+1} = \frac{(2\theta - 1)\gamma_{n+2}^{3/2}}{2(1 + \gamma_{n+2})}\frac{\|\nabla^{-1}(\phi^{n+1} - \phi^n)\|^2}{M\tau_{n+1}} + \frac{\lambda_1}{2\epsilon^2}\|\phi^{n+1}\|^2$$
$$+ \frac{\lambda_2}{2}\|\nabla\phi^{n+1}\|^2 + \frac{\lambda_3}{2}\|\Delta\phi^{n+1}\|^2 + |u^{n+1}|^2.$$

THEOREM 4.4. *The solution of the $\mathcal{V}_L$-method (4.27) satisfies the mass conservation.*

REMARK 4.1. *Taking $\gamma_{n+1} = 1$ in (4.7) and (4.27), the $\mathcal{V}_L$-method and $\mathcal{V}_M$-method can degenerate into their corresponding $\mathcal{U}_L$-method and $\mathcal{U}_W$-method on the uniform temporal mesh. However, the technique for constructing discrete energy in this section requires that $M(\phi)$ be a positive constant or a time-dependent positive function. However, the $\mathcal{U}_L$-method and $\mathcal{U}_M$-method we propose can maintain unconditional energy stability for any $M(\phi)$.*

REMARK 4.2. *Introducing the second order stabilization term, $\phi^{n+1} - (1 + \gamma_{n+1})\phi^n + \gamma_{n+1}\phi^{n-1}$, in the $\mathcal{V}_L$-method and $\mathcal{V}_W$-method, similar to the technique used in the $\mathcal{U}_L$-method and $\mathcal{U}_W$-method, results in our inability to construct discrete energy formulations that preserve unconditional energy stability. Additionally, If we choose to add second-order stabilization terms, such as $\tau(\phi^{n+1} - \phi^n)$ and $\tau^2\phi^{n+1}$, which are easy to construct discrete energy formulations that maintain unconditional energy stability, results in poor stability in practical computation. Therefore, we employ a different technique for adding stabilization terms.*

5. Numerical simulations. In this section, we provide several numerical examples to verify the accuracy, mass conservation and energy dissipation of the proposed schemes. In all the tests, we discretize space using the Fourier spectral method [49, 50, 51].

In the absence of explicit specifications, the parameters for the numerical experiments are set as follows

$$(5.1) \qquad M(\phi) = 1, \epsilon = 0.2, \beta = 6e-4, S_1 = 4, S_2 = 4, \lambda_1 = 0, \lambda_2 = 4.$$

5.1. Numerical simulations in 1D. In this subsection, we perform numerical simulations, include accuracy and structure-preservation of the solutions, for the linear regularization model with $\mathcal{U}_L$-method (3.10) and $\mathcal{V}_L$-method (4.7) in 1D. Here, the computational domain is defined as $\Omega = [0, 2\pi]$, with the mesh size $N_x = 128$.

Example 1. In this example, we aim to test the convergence rates of $\mathcal{U}_L$-method and $\mathcal{V}_L$-method in various parameter settings. To this end, we add a source term in the original model, determined by the exact solution

$$(5.2) \qquad \phi(x, t) = (t+1)^3 \sin(x).$$

Firstly, we plot the L^2-norm errors of the $\mathcal{U}_L$-method in Figure 5.1. We can observe from Figure 5.1 that the error curves of the schemes under $S_1 = 0, S_2 = 0$ and $S_1 = 4, S_2 = 0$ are incomplete, which means that the corresponding schemes are unstable and their solutions may exhibit explosive growth during computation. In addition, the solutions under $S_1 = 0, S_2 = 4$ show better convergence than those under $S_1 = 4, S_2 = 4$ with small time steps due to the introduction of additional error terms when $S_1 = 4$. However, the solutions under $S_1 = 4, S_2 = 4$ consistently maintain good convergence, even with larger time steps, while those under $S_1 = 0, S_2 = 4$ do not. From Figure 5.1, we can also see that as the anisotropy intensity increases, the effect becomes more pronounced. The $\mathcal{V}_L$-method on temporal mesh shows similar numerical results as the $\mathcal{U}_L$-method, see Figure 5.2. From the tests in this example, we conclude that the stabilization terms dramatically influence the convergence of the numerical schemes.

Example 2. In this example, we present the evolutions of the relative mass error defined by $\Delta M(t) = \frac{M(t)-M(0)}{M(0)}$ and the evolutions of the energy function for different values of α and θ. We consider the following two types of initial conditions:

$$(5.3) \qquad \phi(x, 0) = |\sin(x)|,$$

$$(5.4) \qquad \phi(x, 0) = -0.3 + 0.001 rand(x).$$

For various values of the anisotropy intensity parameter α and the weighted parameter θ, the relative errors of mass and the energy for the $\mathcal{U}_L$-method and $\mathcal{V}_L$-method are plotted in Figures 5.3, 5.4, 5.5 and 5.6. We can conclude that both $\mathcal{U}_L$-method and $\mathcal{V}_L$-method can preserve mass conservation and energy dissipation very well, which are consistent with our theoretical analysis.

5.2. Numerical simulations in 2D. In this subsection, we perform numerical simulations, include structure-preservation of the solutions and temporal evolution, for the linear regularization model with $\mathcal{U}_L$-method (3.10) and $\mathcal{V}_L$-method (4.7) in 2D. Here, the computational domain is defined as $\Omega = [0, 2\pi] \times [0, 2\pi]$ with the mesh size $N_x = 128, Ny = 128$.

Example 3. In this example, we numerical simulate the evolution of two circles, and the initial condition is given by

$$(5.5) \qquad \phi(x, y, 0) = \sum_{i=1}^{2} -tanh(\frac{\sqrt{(x-x_i)^2 + (y-y_i)^2} - r_i}{1.2\epsilon}) + 1,$$
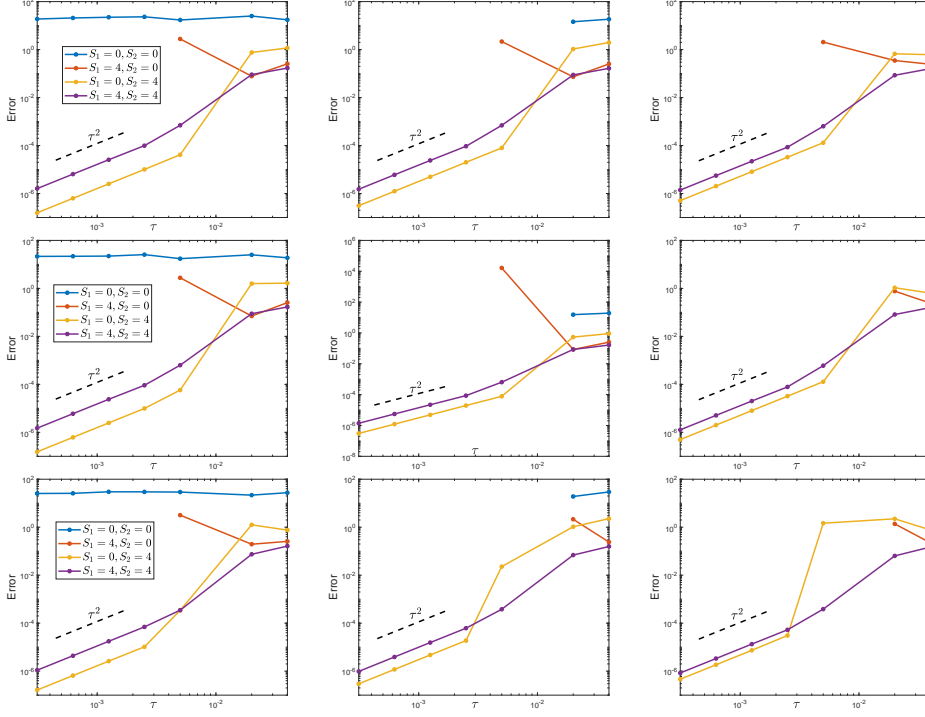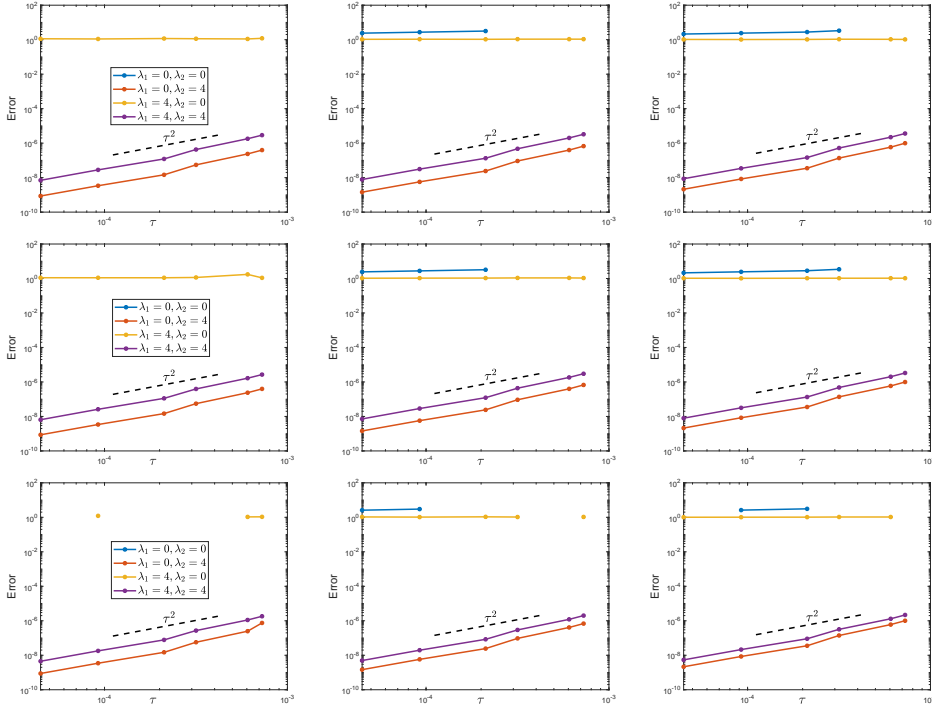
FIG. 5.1. L^2-norm errors for the uniform-time-step method with different θ: $\theta = 0.5$ (first column), $\theta = 0.75$ (second column), $\theta = 1$ (last column), and with different α: $\alpha = 0$ (first row), $\alpha = 0.05$ (second row) and $\alpha = 0.3$ (last row). The other parameters are selected by (5.1).

where $(x_1, y_1, r_1) = (\pi - 0.7, \pi - 0.6, 1.5)$ and $(x_1, y_1, r_1) = (\pi + 1.65, \pi + 1.6, 0.7)$.

In figures 5.7 and 5.8, we plot the relative errors of mass and energy with the initial condition (5.5) for $\mathcal{U}_L$-method and $\mathcal{V}_L$-method. which indicate that both these methods maintain structure-preserving properties. Additionally, snapshots of the profiles of the phase-field variable ϕ with various anisotropy intensity at different times for $\mathcal{U}_L$-method and $\mathcal{V}_L$-method in Figures 5.9 and 5.10. We observe that a coarsening effect in which the smaller circle is absorbed by the larger circle for isotropic system. Furthermore, for isotropic system, the two circles initially evolve into anisotropic shapes, missing orientation at the four corners, followed by the coarsening of the anisotropic system, resulting in the disappearance of the smaller shape. In addition, as the intensity of anisotropy increases, the equilibrium shapes tend to become pyramids with sharper angles from the Figures 5.9 and 5.10.

Example 4. In this example, we adopt a random initial condition to simulate the free energy evolution of both an isotropic model and an anisotropic model, and present the temporal evolution of the solutions. Here, we use $\mathcal{U}_L$-method for numerical simulation, and the following random initial condition is chosen below:

$$(5.6) \qquad \phi(x, y, 0) = -0.5 + 0.001 rand(x, y).$$

We set the time step $\tau = 5e-2$ with the weighted parameter $\theta = 0.75$, and select the other parameters by (5.1). For isotropic system, from Figure 5.11, we can observe that snapshot of solution with random initial value evolve into multiple circles following the first rapid decline in free energy function. After the second rapid decline, the free energy function reaches a steady state, and the snapshots transform into a single circle. Additionally, in Figure 5.12,

FIG. 5.2. L^2-norm errors for the variable-time-step method with different θ: $\theta = 0.5$ (first column), $\theta = 0.75$ (second column), $\theta = 1$ (last column), and with different α: $\alpha = 0$ (first row), $\alpha = 0.05$ (second row) and $\alpha = 0.3$ (last row). The other parameters are selected by (5.1).
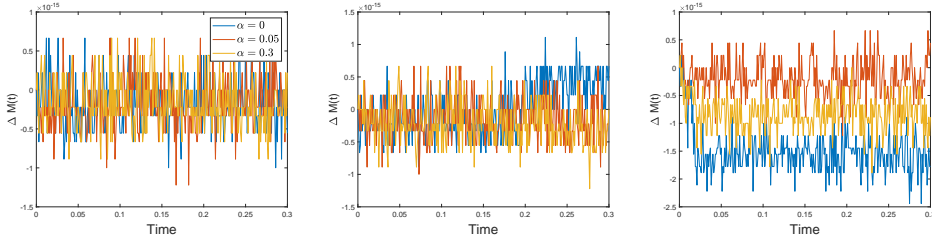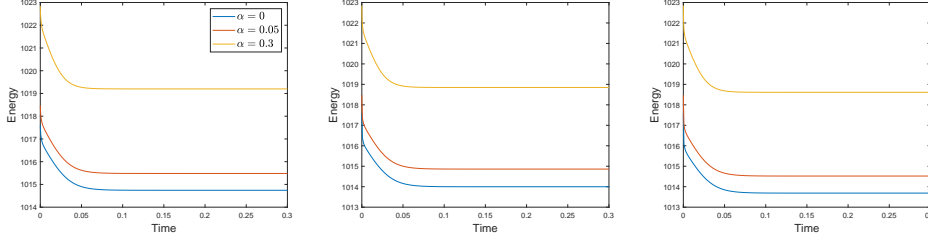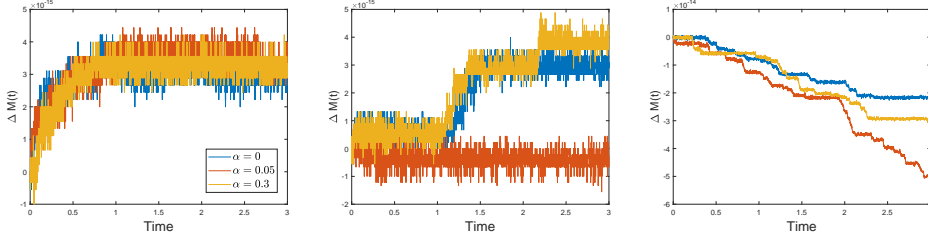

(a) The relative errors of mass.
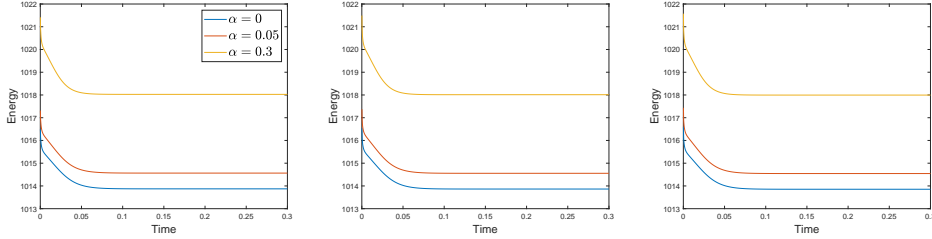
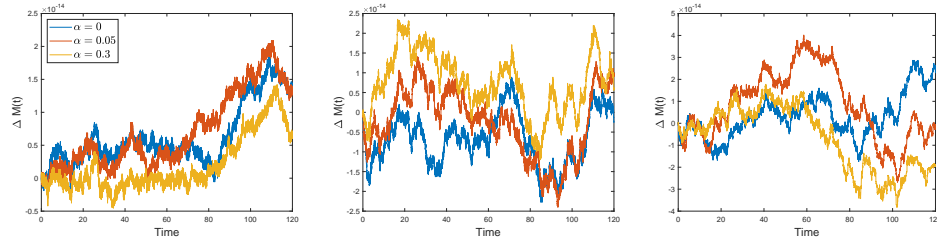(b) The energy evolutions.

FIG. 5.3. The relative error of mass and the energy evolutions for $\mathcal{U}_L$-method with different θ: $\theta = 0.5$ (first column), $\theta = 0.75$ (second column), $\theta = 1$ (last column). The initial condition is chosen as (5.3) and the other parameters are selected by (5.1). (a) The relative error of mass with $\tau = 1e - 3$. (b) The modified energy (3.14) with $\tau = 1e - 3$.
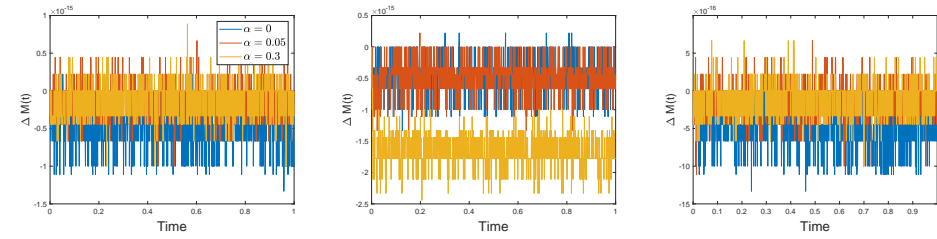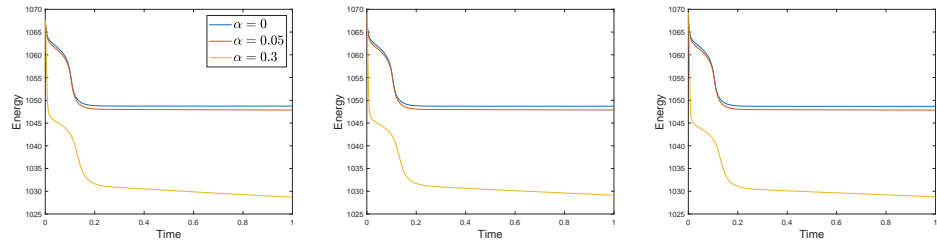
18
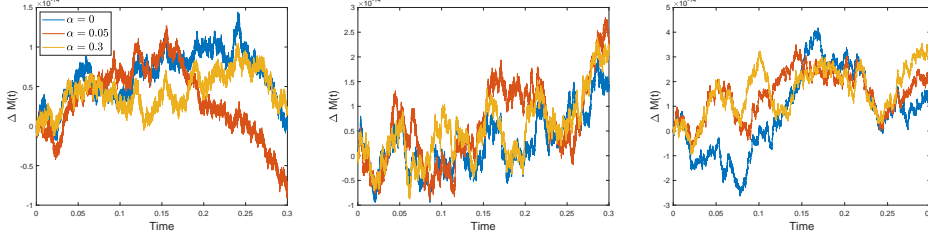
(a) The relative errors of mass.

(b) The energy evolutions.

FIG. 5.4. *The relative error of mass and the energy evolutions for $\mathcal{V}_L$-method with different θ: $\theta = 0.5$ (first column), $\theta = 0.75$ (second column), $\theta = 1$ (last column). The initial condition is chosen as (5.3) and the other parameters are selected by (5.1). (a) The relative error of mass with $\tau_{max} = 1.0165e - 4$. (b) The modified energy (4.15) with $\tau_{max} = 1.0165e - 4$.*
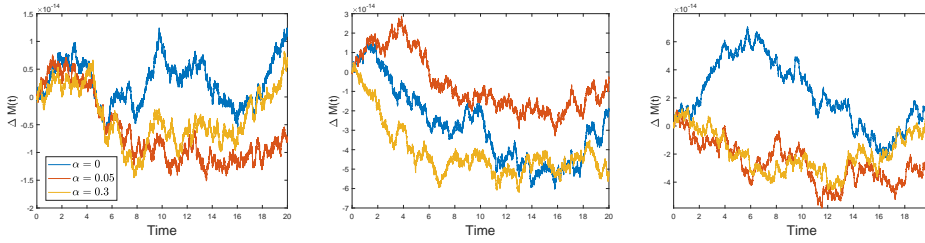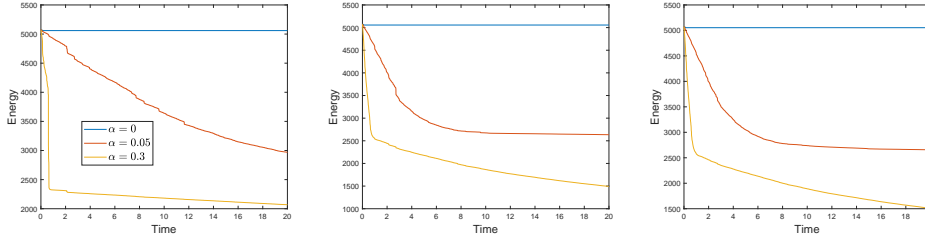

(a) The relative error of mass.
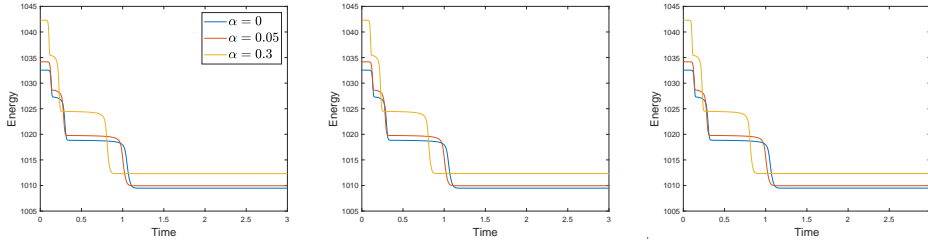
(b) The energy evolutions.

FIG. 5.5. *The relative error of mass and the energy evolutions for $\mathcal{U}_L$-method with different θ: $\theta = 0.5$ (first column), $\theta = 0.75$ (second column), $\theta = 1$ (last column). The random initial condition (5.4) is chosen and the other parameters are selected by (5.1). (a) The relative error of mass with $\tau = 1e - 3$. (b) The modified energy (4.15) with $\tau = 1e - 3$.*

We see the combined effects of anisotropy and coarsening as time evolves. The free energy function undergoes multiple rapid declines to reach a steady state. Ultimately, the snapshot

(a) The relative error of mass.
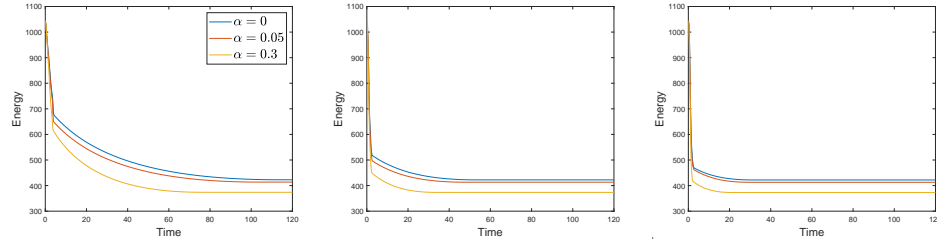
(b) The energy evolutions.

Fig. 5.6. *The relative error of mass and the energy evolutions for $\mathcal{V}_L$-method with different θ: $\theta = 0.5$ (first column), $\theta = 0.75$ (second column), $\theta = 1$ (last column). The random initial condition (5.4) is chosen and the other parameters are selected by (5.1). (a) The relative error of mass with $\tau_{max} = 1.0165e - 4$. (b) The modified energy (4.15) with $\tau_{max} = 1.0165e - 4$.*

(a) The relative error of mass.

(b) The energy evolutions.

Fig. 5.7. *The relative error of mass and the energy evolutions for $\mathcal{U}_L$-method with different θ: $\theta = 0.5$ (first column), $\theta = 0.75$ (second column), $\theta = 1$ (last column). The random initial condition (5.4) is chosen and the other parameters are selected by (5.1). (a) The relative error of mass with $\tau = 1e - 3$. (b) The modified energy (4.15) with $\tau = 1e - 3$.*

of ϕ evolve into a pyramid at the steady state.

(a) The relative error of mass.

(b) The energy evolutions.

Fig. 5.8. *The relative error of mass and the energy evolutions for $\mathcal{V}_L$-method with different θ: $\theta = 0.5$ (first column), $\theta = 0.75$ (second column), $\theta = 1$ (last column). The random initial condition (5.4) is chosen and the other parameters are selected by (5.1). (a) The relative error of mass with $\tau = 1e - 3$. (b) The modified energy (4.15) with $\tau = 1e - 3$.*

6. Conclusions. In this work, we have proposed WSBDF2 method combined stabilization technique on uniform/nonuniform temporal mesh to solve anisotropic CH models with linear and Willmore regularization, respectively. On uniform temporal mesh, we have employed uniform-time-step WSBDF2 method combined with the traditional SAV approach, and different numerical schemes can be obtained by adjusting the weighted parameter θ. Compared to th existing uniform numerical methods for anisotropic CH models, the proposed WSBDF2 scheme on nonuniform temporal mesh not only well capture the dynamics of the solutions as well as provide a new approach to easily adopt adaptive time stepping methods in future, but also deduce different schemes by change the value of parameter θ. Moreover, the structure-preserving properties of our proposed schemes are rigorously proved. Finally, extensive numerical experiments validate the correctness and effectiveness of the proposed schemes in theory.

REFERENCES

[1] A. R tz, A. Ribalta, A. Voigt, Surface evolution of elastically stressed films under deposition by a diffuse interface model, Journal of Computational Physics 214 (1) (2006) 187–208.

[2] J. Eggleston, P. Voorhees, Ordered growth of nanocrystals via a morphological instability, Applied Physics Letters 80 (2) (2002) 306–308.

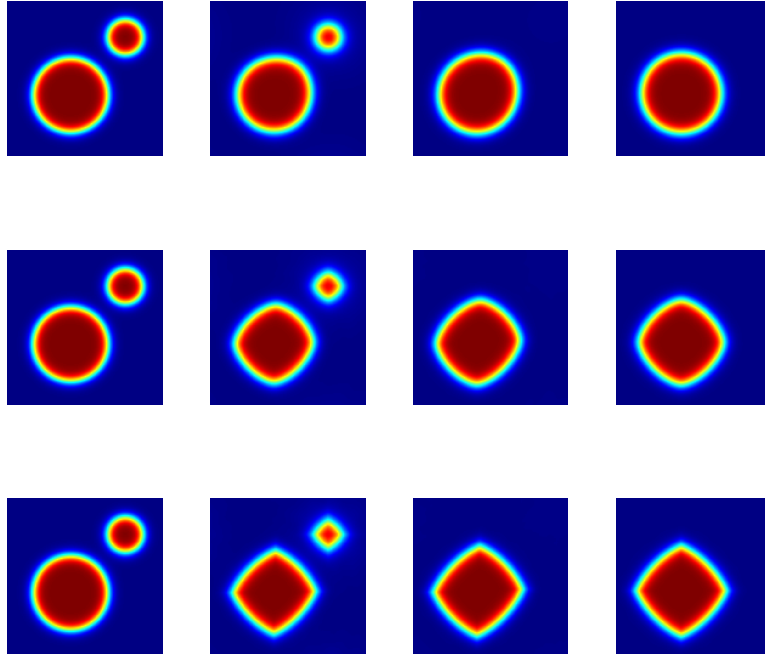[3] S. Wise, J. Lowengrub, J. Kim, K. Thornton, P. Voorhees, W. Johnson, Quantum dot formation on a strain-

Fig. 5.9. *Snapshots of ϕ are taken at $0, 6.5e-2, 1.99e-1$ and 2 for $\mathcal{U}_L$-method with $\tau = 1e-3$. The weighted parameter $\theta = 0.75$ and the other parameters are selected by (5.1). (a) The 2D dynamical evolution of the phase variable ϕ with $\alpha = 0$. (b) The 2D dynamical evolution of the phase variable ϕ with $\alpha = 0.05$. (c) The 2D dynamical evolution of the phase variable ϕ with $\alpha = 0.1$.*

patterned epitaxial thin film, Applied Physics Letters 87 (13).

[4] J. Erlebacher, M. J. Aziz, A. Karma, N. Dimitrov, K. Sieradzki, Evolution of nanoporosity in dealloying, Nature 410 (6827) (2001) 450–453.

[5] F. Campelo, A. Hernandez-Machado, Dynamic model and stationary shapes of fluid vesicles, The European Physical Journal E 20 (2006) 37–45.

[6] A. C. Aristotelous, O. A. Karakashian, S. M. Wise, Adaptive, second-order in time, primitive-variable discontinuous galerkin schemes for a Cahn–Hilliard equation with a mass source, IMA Journal of Numerical Analysis 35 (3) (2015) 1167–1198.

[7] H. B. Frieboes, J. S. Lowengrub, S. Wise, X. Zheng, P. Macklin, E. L. Bearer, V. Cristini, Computer simulation of glioma growth and morphology, Neuroimage 37 (2007) S59–S70.

[8] J. Lowengrub, L. Truskinovsky, Quasi–incompressible Cahn–Hilliard fluids and topological transitions, Proceedings of the Royal Society of London. Series A: Mathematical, Physical and Engineering Sciences 454 (1978) (1998) 2617–2654.

[9] J. Kim, K. Kang, J. Lowengrub, Conservative multigrid methods for Cahn–Hilliard fluids, Journal of Computational Physics 193 (2) (2004) 511–543.

[10] V. E. Badalassi, H. D. Ceniceros, S. Banerjee, Computation of multiphase systems with phase field models, Journal of Computational Physics 190 (2) (2003) 371–397.

[11] I. Klapper, J. Dockery, Role of cohesion in the material description of biofilms, Physical Review E 74 (3) (2006) 031902.

[12] A. L. Bertozzi, S. Esedoglu, A. Gillette, Inpainting of binary images using the Cahn–Hilliard equation, IEEE Transactions on Image Processing 16 (1) (2006) 285–291.

[13] I. C. Dolcetta, S. F. Vita, R. March, Area-preserving curve-shortening flows: from phase separation to image processing, Interfaces and Free Boundaries 4 (4) (2002) 325–343.

[14] V. Chalupeckỳ, Numerical studies of Cahn–Hilliard equation and applications in image processing, in: Proceedings of Czech–Japanese Seminar in Applied Mathematics, 2004.
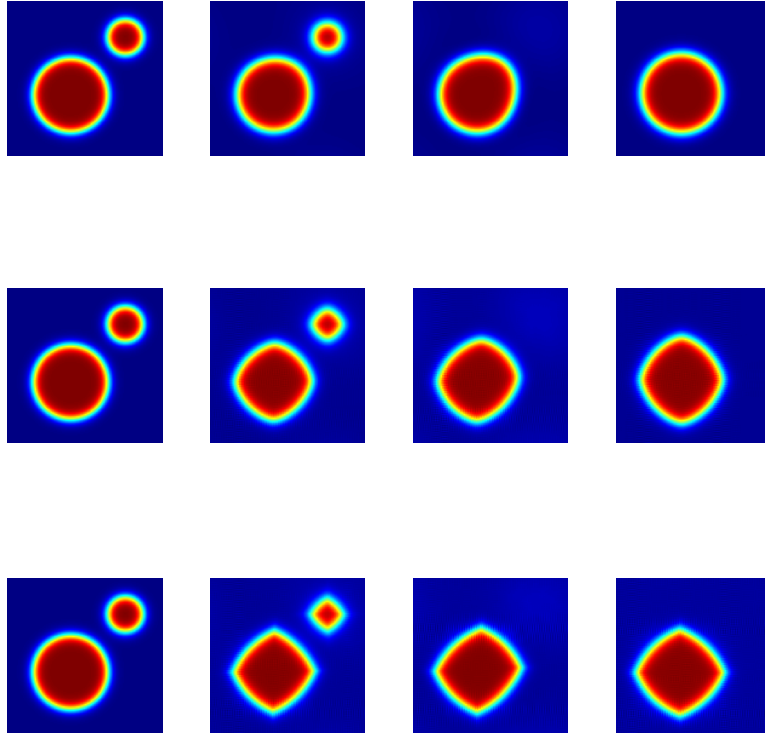
Fig. 5.10. *Snapshots of ϕ, for $\mathcal{V}_L$-method, are taken at $0, 6.5e-2, 1.99e-1$ and 2 with $\tau = 1e-3$, where initial condition (5.6). The weighted parameter $\theta = 0.75$ and the other parameters are selected by (5.1). (a) The 2D dynamical evolution of the phase variable ϕ with $\alpha = 0$. (b) The 2D dynamical evolution of the phase variable ϕ with $\alpha = 0.05$. (c) The 2D dynamical evolution of the phase variable ϕ with $\alpha = 0.1$.*

[15] A. Miranville, The Cahn–Hilliard equation: recent advances and applications, SIAM, 2019.

[16] A. Novick-Cohen, The Cahn–Hilliard equation, Handbook of differential equations: evolutionary equations 4 (2008) 201–228.

[17] Q. Du, L. Ju, X. Li, Z. Qiao, Maximum principle preserving exponential time differencing schemes for the nonlocal Allen–Cahn equation, SIAM Journal on numerical analysis 57 (2) (2019) 875–898.

[18] Q. Du, L. Ju, X. Li, Z. Qiao, Maximum bound principles for a class of semilinear parabolic equations and exponential time-differencing schemes, SIAM Review 63 (2) (2021) 317–359.

[19] S. Wise, J. Kim, J. Lowengrub, Solving the regularized, strongly anisotropic Cahn–Hilliard equation by an adaptive nonlinear multigrid method, Journal of Computational Physics 226 (1) (2007) 414–446.

[20] S. Torabi, J. Lowengrub, A. Voigt, S. Wise, A new phase-field model for strongly anisotropic systems, Proceedings of the Royal Society A: Mathematical, Physical and Engineering Sciences 465 (2105) (2009) 1337–1359.

[21] F. Chen, J. Shen, Efficient energy stable schemes with spectral discretization in space for anisotropic Cahn–Hilliard systems, Communications in Computational Physics 13 (5) (2013) 1189–1208.

[22] J. Shen, J. Xu, Stabilized predictor-corrector schemes for gradient flows with strong anisotropic free energy, Communications in Computational Physics.

[23] C. Chen, X. Yang, Fast, provably unconditionally energy stable, and second-order accurate algorithms for the anisotropic Cahn–Hilliard model, Computer Methods in Applied Mechanics and Engineering 351 (2019) 35–59.

[24] Z. Xu, X. Yang, H. Zhang, Z. Xie, Efficient and linear schemes for anisotropic Cahn–Hilliard using the stabilized-invariant energy quadratization (S-IEQ) approach, Computer Physics Communications 238 (2019) 36–49.
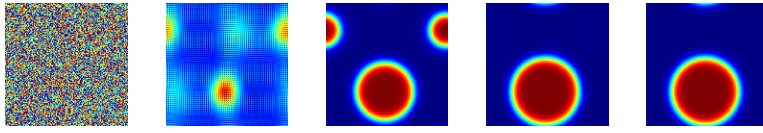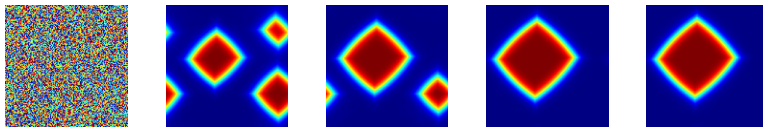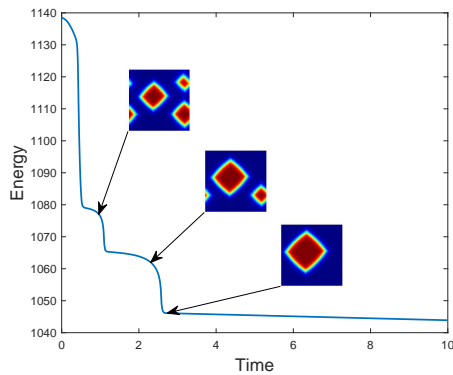
(a) Snapshots of φ.
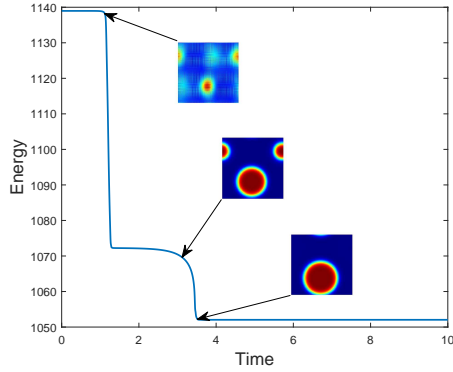
(b) Evolutions of free energy

Fɪɢ. 5.11. *(a) The 2D dynamical evolution of the phase variable φ for the isotropic model (α = 0) with the linear regularization with the random initial condition 5.6, and snapshots are taken at* 0, 1.115, 3.12, 3.52 *and* 10. *(b) Time evolution of the free energy* (3.14).

(a) Snapshots of φ.

(b) Evolutions of free energy

Fɪɢ. 5.12. *(a) The 2D dynamical evolution of the phase variable φ for the anisotropic model (α = 0.2) with the linear regularization with the random initial condition 5.6, and snapshots are taken at* 0, 0.965, 2.31, 2.74 *and* 10. *(b) Time evolution of the free energy* (3.14).

[25] E. Hairer, G. wanner solving ordinary differential equations 2-stiff and differential algebraic equations (1996).

[26] H. Gomez, T. J. Hughes, Provably unconditionally stable, second-order time-accurate, mixed variational methods for phase-field models, Journal of Computational Physics 230 (13) (2011) 5310–5327.

[27] H.-L. Liao, X. Song, T. Tang, T. Zhou, Analysis of the second-order BDF scheme with variable steps for the molecular beam epitaxial model without slope selection, Science China Mathematics 64 (2021) 887–902.

[28] Z. Qiao, Z. Zhang, T. Tang, An adaptive time-stepping strategy for the molecular beam epitaxy models, SIAM Journal on Scientific Computing 33 (3) (2011) 1395–1414.

[29] Z. Zhang, Z. Qiao, An adaptive time-stepping strategy for the Cahn-Hilliard equation, Communications in Computational Physics 11 (4) (2012) 1261–1278.

[30] Y. Di, Y. Wei, J. Zhang, C. Zhao, Sharp error estimate of an implicit BDF2 scheme with variable time steps for the phase field crystal model, Journal of Scientific Computing 92 (2) (2022) 65.

[31] J. Zhang, C. Zhao, Sharp error estimate of BDF2 scheme with variable time steps for molecular beam epitaxial models without slop selection, Journal of Mathematics 42 (5) (2022) 377–401.

[32] R. D. Grigorieff, Stability of multistep-methods on variable grids, Numerische Mathematik 42 (1983) 359–377.

[33] J. Becker, A second order backward difference method with variable steps for a parabolic problem, BIT Numerical Mathematics 38 (1998) 644–662.

[34] W. Chen, X. Wang, Y. Yan, Z. Zhang, A second order BDF numerical scheme with variable steps for the Cahn–Hilliard equation, SIAM Journal on Numerical Analysis 57 (1) (2019) 495–525.

[35] H.-l. Liao, Z. Zhang, Analysis of adaptive BDF2 scheme for diffusion equations, Mathematics of Computation 90 (329) (2021) 1207–1226.

[36] J. Zhang, C. Zhao, Sharp error estimate of BDF2 scheme with variable time steps for linear reaction-diffusion equations, Journal of Mathematics 41 (6) (2021) 471–488.

[37] D. Hou, Z. Qiao, An implicit–explicit second-order BDF numerical scheme with variable steps for gradient flows, Journal of Scientific Computing 94 (2) (2023) 39.

[38] H.-l. Liao, D. Li, J. Zhang, Sharp error estimate of the nonuniform L1 formula for linear reaction-subdiffusion equations, SIAM Journal on Numerical Analysis 56 (2) (2018) 1112–1133.

[39] W. Wang, M. Mao, Z. Wang, Stability and error estimates for the variable step-size BDF2 method for linear and semilinear parabolic equations, Advances in Computational Mathematics 47 (1) (2021) Paper No. 8, 28.

[40] M. Chen, F. Yu, Q. Zhang, Weighted and shifted BDF2 methods on variable grids, arXiv preprint arXiv:2108.02910.

[41] G. Akrivis, M. Chen, J. Han, F. Yu, Z. Zhang, The variable two-step BDF method for parabolic equations, BIT Numerical Mathematics 64 (1) (2024) 14.

[42] Q. Liu, J. Jing, M. Yuan, W. Chen, A positivity-preserving, energy stable BDF2 scheme with variable steps for the Cahn–Hilliard equation with logarithmic potential, Journal of Scientific Computing 95 (2) (2023) 37.

[43] M. Li, L. Wang, N. Wang, Variable-time-step BDF2 nonconforming VEM for coupled Ginzburg-Landau equations, Applied Numerical Mathematics 186 (2023) 378–410.

[44] N. Wang, M. Li, Unconditional error analysis of a linearized BDF2 virtual element method for nonlinear Ginzburg–Landau equation with variable time step, Communications in Nonlinear Science and Numerical Simulation 116 (2023) 106889.

[45] Z. Zhang, Y. Ma, Z. Qiao, An adaptive time-stepping strategy for solving the phase field crystal model, Journal of Computational Physics 249 (2013) 204–215.

[46] F. Huang, J. Shen, Z. Yang, A highly efficient and accurate new scalar auxiliary variable approach for gradient flows, SIAM Journal on Scientific Computing 42 (4) (2020) A2514–A2536.

[47] J. Shen, J. Xu, J. Yang, The scalar auxiliary variable (SAV) approach for gradient flows, Journal of Computational Physics 353 (2018) 407–416.

[48] H.-l. Liao, B. Ji, L. Wang, Z. Zhang, Mesh-robustness of an energy stable BDF2 scheme with variable steps for the Cahn–Hilliard model, Journal of Scientific Computing 92 (2) (2022) 52.

[49] J. Shen, T. Tang, L.-L. Wang, Spectral methods: algorithms, analysis and applications, Vol. 41, Springer Science & Business Media, 2011.

[50] M. Ainsworth, Z. Mao, Analysis and approximation of a fractional Cahn–Hilliard equation, SIAM Journal on Numerical Analysis 55 (4) (2017) 1689–1718.

[51] S. Chen, J. Shen, Enriched spectral methods and applications to problems with weakly singular solutions, Journal of Scientific Computing 77 (3) (2018) 1468–1489.